



U.S. DEPARTMENT OF THE INTERIOR
U.S. GEOLOGICAL SURVEY

**PRELIMINARY GEOPHYSICAL FRAMEWORK OF THE UPPER AND MIDDLE
VERDE RIVER WATERSHED, YAVAPAI COUNTY, ARIZONA**

Victoria E. Langenheim¹, Ed DeWitt², and Laurie Wirt²

¹U.S. Geological Survey, 345 Middlefield Road, Menlo Park, CA 94025

²U.S. Geological Survey, Box 25046, Denver Federal Center, Denver, CO 80225

Open-File Report 2005-1154

2005



This report is preliminary and has not been reviewed for conformity with U.S. Geological Survey editorial standards or with the North American Stratigraphic Code. Any use of trade, firm, or product names is for descriptive purposes only and does not imply endorsement by the U.S. Government.

PRELIMINARY GEOPHYSICAL FRAMEWORK OF THE UPPER AND MIDDLE VERDE RIVER WATERSHED, YAVAPAI COUNTY, ARIZONA

Victoria E. Langenheim, Ed DeWitt, and Laurie Wirt

ABSTRACT

Analysis of aeromagnetic and gravity data provides new insights into the geometry of geologic structures of the upper and middle Verde River watershed, Yavapai County, Arizona. Magnetic anomalies reveal hidden volcanic rocks lying at shallow depths beneath the ground surface in Williamson, Little Chino, Big Chino and Verde Valleys in the upper Verde River watershed, Yavapai County, Arizona. Concentrations of shallowly buried volcanic plugs or centers are located down-gradient of springs (Del Rio) and perennial flow (Williamson Valley), suggesting that these volcanic centers or plugs may retard ground-water flow. Magnetic data also map paleo-channels filled with 4-6 Ma basalt as Big Chino Valley formed and subsided during late Tertiary time. The magnetic data reveal a predominantly northeast-to north-striking structural grain within Proterozoic basement rocks, in contrast to the generally northwest strike of late Tertiary faults in this region. The magnetic grain may serve as a proxy for fracturing and faulting, an important source of permeability in these generally impermeable rocks. Magnetic and gravity data also delineate exposed and concealed faults within the study area. The Big Chino fault and Verde fault zone have the largest amounts of vertical throw of any fault in the study area based on gravity, magnetic, and limited well data. These faults bound deep (1-2 km) basins in Big Chino and Verde Valleys. The geophysical data also reveal concealed faults in Williamson Valley that bound a previously undiscovered basin with approximately 1 km of Cenozoic fill inferred from inversion of gravity data. Little Chino and Lonesome Valleys, including the upper reach of the Agua Fria basin, are characterized by basin fill which nowhere exceeds 1 km and has a more irregular distribution with local, north-to northwest-striking pockets of thicker sediment. A 15- to 20-km-long northwest-striking magnetic lineament that passes through Page Springs in Verde Valley can be used to project a fault 5-10 km northwest and southeast of its mapped trace. The collocation of the lineament, mapped fault, and the spring suggests structural influence on the location of this large spring.

CONVERSION FACTORS AND ABBREVIATIONS

Conversion factors

Multiply	By	To obtain
	Length	
meter (m)	3.2808	foot (ft)
kilometer (km)	0.621	mile (mi)
	Area	
square kilometer (km ²)	0.386	square mile (mi ²)

Abbreviations

cgs unit	centimeter-grams-second unit (magnetic susceptibility)
emu/cc	electromagnetic unit/cubic centimeter (magnetization)
g/cm ³	grams per cubic centimeter (density)
Ma	million years (time)

Cover photo: A view of the Verde River, north of Clarkdale, Arizona. Red, well bedded rocks in background are nearly horizontal beds of the Supai Formation.

INTRODUCTION

Yavapai County, Arizona is one of the fastest-growing rural counties in the United States, with population growth concentrated in Verde Valley, the Prescott area, and Sedona (Fig. 1). Rapid population growth has led to a concurrent increase in water-resources development. Although the Verde River provides surface water to water-rights holders in Verde Valley and Phoenix, ground water is the major source of most public and domestic water supplies in Yavapai County according to the Arizona Department of Water Resources (2000). In order to improve understanding of the geologic framework and its effect on ground-water flow, the county contracted the U.S. Geological Survey to conduct geophysical and geologic studies to aid construction of a ground-water flow model of the region.

The goal of this study is to improve understanding of the geologic framework of the upper Verde River region (Fig. 1) from analysis of geophysical data. This work builds upon earlier geohydrologic studies (Twenter and Metzger, 1963; Owen-Joyce and Bell, 1983; Water Resources Associates, 1989; Ostenaar and others, 1993) and geologic studies (Krieger, 1965; DeWitt and others, in press) that focused on geologic mapping and water well information. This study concentrates on projecting surficial structures and stratigraphy into the subsurface using geophysical data. This includes a more quantitative and detailed interpretation of aeromagnetic and gravity data collected by the U.S. Geological Survey in 1999-2001 than that outlined in Langenheim and others (2000, 2002) and expands the area of interpretation beyond that presented in Langenheim and others (2005). The isostatic gravity anomaly data reflect density variations in the upper and middle crust. Interpretation of these anomalies provides information on the depth of Cenozoic basins and on the nature of pre-Cenozoic basement rocks. The aeromagnetic data are sensitive to the distribution of magnetic rocks, primarily those containing magnetite. In Yavapai County, these rocks are Tertiary volcanic and certain rock types within the Proterozoic crystalline basement. In particular, aeromagnetic anomalies mark abrupt spatial contrasts in magnetization that can be attributed to lithologic boundaries, often caused by faulting and fracturing of these rocks. These two geophysical datasets, in concert with information from geologic mapping, wells, and other types of geophysical data, are effective tools in defining hidden structures important to ground-water studies, such as the configuration and structural fabric of basement and distribution of volcanic rocks concealed beneath Tertiary sedimentary deposits.

GEOLOGIC SETTING

The study area lies within the transition zone between the Colorado Plateaus and the Basin and Range physiographic provinces and includes much of Yavapai County (Fig. 1). The transition zone exhibits geologic features common to both provinces. For example, regional projections indicate that Paleozoic strata are nearly continuous across the Colorado Plateaus-transition zone boundary with a regional dip of $<10^\circ$ northward toward the plateau (Twenter and Metzger, 1963). This regional dip is interrupted by steeper dips associated with monoclines (Krieger, 1965). The zone is also characterized by a series of Tertiary and Quaternary north- and northwest-striking normal faults (Menges and Pearthree, 1983; Reynolds, 1988), which are characteristic of the Basin and Range province to the south.

Rock Types

Rocks exposed in the study area consist of four main types and ages. Early and Middle Proterozoic plutonic and metamorphic rocks constitute the basement of the mountains and

valleys in the region. Basement exposures are abundant in the Bradshaw and Juniper Mountains and the Black Hills (Fig. 2). Distribution of basement rocks is important because the plutonic and metamorphic units typically have very low permeability (except through interconnected fractures) and thus are generally poor aquifers. Paleozoic sedimentary rocks overlie the basement and are exposed throughout the area except where removed by erosion during Tertiary (maybe Cretaceous?) time or where buried by younger rocks or alluvium. Rock types include sandstone, limestone, dolomite, and minor shale, which together constitute what is termed the regional carbonate aquifer. Tertiary volcanic rocks are locally abundant both in mountain ranges and within the basins. Depending on composition and texture, volcanic rocks can have a wide range of permeability and either can transmit water readily or retard its flow. Tertiary to Quaternary sediments and rocks are abundant in the valleys, and form the basin-fill aquifers. These rocks can be important aquifers and include fanglomerate, varied alluvial deposits, and playa deposits, all of which interfinger, creating locally complex depositional patterns and highly heterogeneous permeabilities.

Proterozoic igneous and metamorphic rocks are exposed in the mountain ranges that lie along the southern (Bradshaw Mountains) and western (Juniper and Santa Maria Mountains) fringes of the study area (Anderson and Blacet, 1972a; Fig. 2). Proterozoic rocks also are extensively exposed in the Black Hills in the south-central part of the study area. Isolated Proterozoic metasedimentary, metavolcanic and igneous rocks also are exposed in the area (e.g., 2 km east of Del Rio Springs, 5 km west of Sullivan Buttes, where the Verde fault intersects the Verde River, and the outcrops at the northern end of the Big Chino fault; Figs. 1 and 2). These basement rocks are compositionally very heterogeneous, ranging from mafic (gabbro and metabasalt) to felsic (metarhyolite, alaskite, and quartzite). Intruding these basement rocks are Lower Cretaceous tonalite stocks in the Bradshaw Mountains, one of which crops out along the southern border of the geophysical survey 5 km (3.1 mi) west of Highway 69. A possible buried stock is suggested by boulders of granodiorite in sedimentary rocks along the Verde Fault, east of Cherry (DeWitt and others, in press). These Cretaceous stocks are included with the Proterozoic rocks as part of the basement.

The Proterozoic rocks are overlain by Cambrian to Permian sedimentary rocks, throughout much of the area, although the Paleozoic rocks have been stripped away in much of Lonesome Valley, the upper part of the Agua Fria basin, the Bradshaw Mountains, and parts of the Black Hills (Krieger, 1965). The thickness of the Paleozoic sequence ranges from zero in parts of the Black Hills, Bradshaw Mountains, and Little Chino Valley to as much as 1,330 m (4,375 feet) in the northern parts of the study area. Triassic sedimentary rocks (Moenkopi Formation) are present in far north-central part of area, along the Mogollon Rim, near Sycamore Canyon (Fig. 1).

A major unconformity and long period of erosion separate the Proterozoic, Paleozoic and Mesozoic rocks from Tertiary and Quaternary sedimentary and volcanic rocks. Quaternary deposits include alluvial fans, colluvium covering hill slopes, floodplain terraces, and stream gravels. In the center of the valleys, these young Quaternary deposits are commonly less than 15 m (50 ft) thick. Thick alluvial fan deposits are prevalent along the valley margins. For example, some of the largest fans along Big Black Mesa are at least 150 m (500 ft) thick (Ostenaar and others, 1993).

Tertiary (Oligocene? to Pliocene) sedimentary rocks are extensively exposed in the valley areas. Along the margins of Lonesome Valley, Tertiary fanglomerate, mud flow deposits, and tuffaceous deposits are exposed; towards the interior of the basin, these rocks also include

channel gravel, sand, silt, clay and marl. Tertiary sedimentary rocks both underlie and overlie, and in places, are interbedded with, Tertiary volcanic rocks.

Tertiary volcanic rocks consist of two main lithologies, latite andesite and basalt. Latite andesite, ranging in age from 21-27 Ma, is extensively exposed at Sullivan Buttes (Tyner, 1984). The latite andesite forms a volcanic field that overlies a dissected surface underlain by rocks ranging in age from the Early Proterozoic Mazatzal Group through the Mississippian to Permian Supai Group to Tertiary gravels (Krieger, 1965; DeWitt and others, in press). The lateral extent of the volcanic field is larger than suggested by surficial deposits. Parts of the volcanic field is buried beneath the northern part of Little Chino and Lonesome Valleys and occupy a considerable part of the southeastern part of Big Chino Valley based on interpretation of aeromagnetic data (Langenheim and others, 2000; Langenheim and others, 2005). Outcrops of latite andesite and related rocks to the west of Big Chino Valley, in the Camp Wood area (Ash, 1997), suggest continuity of the volcanic field across much of Williamson Valley and parts of southern Big Chino Valley (DeWitt and others, in press).

Tertiary basalt is exposed in many places throughout the study area and underlies much of Lonesome and Verde Valleys. The basalts are divided into two main sequences (McKee and Anderson, 1971). The older sequence, the Hickey Formation, consists of 10-15 Ma basalt flows and minor interbedded sedimentary rocks as much as 300 m (980 ft) thick. The interbedded sedimentary rocks were derived from the Basin and Range province, to the southwest and include distinctive clasts of Proterozoic basement rocks exposed in the Bradshaw Mountains. The younger sequence consists of 4-7 Ma basalt flows and interbedded conglomeratic sedimentary rocks derived from the Colorado Plateaus to the north, including the so-called "ramp" basalts that flowed into Verde Valley and basalts that flowed into the northern and southern ends of Big Chino Valley. Interbedded sedimentary rocks constitute a significant part of the total thickness of the sequence.

The thickness of the volcanic rocks in the Hickey Formation varies from 0-400 m (0-1300 ft) in the Black Hills (Anderson and Creasey, 1958). Well log data in Lonesome Valley suggest that the upper surface of the volcanic rocks ("malpais" or "malapais" in driller's logs and inferred to be basalt) slopes gently to the southwest from the northeast side of the basin (Krieger, 1965). The maximum thickness of the basalt penetrated in wells in Lonesome Valley is 150 m (500 ft).

In Verde Valley, Tertiary volcanic rocks of the Hickey Formation are overlain by the lakebed deposits of the Miocene to Pliocene Verde Formation (Jenkins, 1923; Lehner, 1958; Twenter and Metzger, 1963; Nations and others, 1981; Holm and others, 1998; Leighty, 1998). These rocks were deposited in a valley similar in size to the present Verde Valley and consist of limestone, mudstone, sandstone, and, locally, evaporite deposits. The exposed thickness of the Verde Formation is about 480 m, but the thickness of the entire formation may exceed 950 m (Nations and others, 1981; DeWitt and others, in press). Playa deposits constitute much of the sedimentary sequence underlying Big Chino Valley (Ostenaa and others, 1993; DeWitt and others, 2005), in contrast with the coarser-grained deposits found in deep drill holes in Williamson Valley.

Structure

The most intense and complexly deformed rocks in the area are the Proterozoic rocks (Anderson and Creasey, 1958; Anderson and Blacet, 1972a, b; Anderson, 1989; DeWitt, 1987,

1989; Wilson, 1939). These rocks have been regionally metamorphosed during Early Proterozoic time to greenschist facies and deformed, and possess a northeast-striking foliation that dips steeply. Zones of high strain are locally apparent in the metamorphic rocks. This deformation did not affect the Paleozoic sequence.

Paleozoic rocks generally dip less than 10° to the northeast in the study area, except near monoclines, such as the Limestone Canyon monocline on Big Black Mesa. The local dip of Paleozoic strata on Big Black Mesa and the area north of the Verde River is probably the result of deformation related to monocline formation. Such deformation resulted in a series of basement-cored blocks that dip gently to the northeast and that are bounded by the northwest-striking monoclines. Paleozoic rocks therefore were stripped from the basement in the southern part of the study area. The age of these monoclines is probably Late Cretaceous to early Tertiary based on their similarity in structure to Laramide monoclines on the Colorado Plateaus (Davis, 1978).

Oligocene (?) to Miocene gravels exposed in the headwaters area of the Verde River are evidence for a northeast-sloping paleo-erosion surface (Elston and Young, 1991). Remnants of these gravels exposed elsewhere suggest that this erosional surface developed before the older sequence of basalts (or latites) erupted. Later extensional faulting resulted in large-scale downdropping of Tertiary volcanic and sedimentary rocks in Verde and Big Chino Valleys starting at about 11-8 Ma (Elston and others, 1974; Elston and Young, 1991; DeWitt and others, in press). Faulting probably continued to 1 Ma. Presumably, faulting also occurred west of the Black Hills at about the same time. Basalts flowed over the resultant escarpments and into valleys in selected places.

Several faults in the Transition zone may show evidence of multiple ages of movement. Shoemaker and others (1978) show several northeast- and northwest-striking fault systems in northwestern Arizona that are Tertiary in age and parallel the Precambrian structural grain. A fault system identified by Krieger (1965) and Shoemaker and others (1978) is the northwest-striking Big Chino fault, exposed along the southwestern edge of Big Black Mesa (Figs. 1, 2). This fault clearly shows evidence of movement as young as Quaternary (Menges and Pearthree, 1983) with 8-10-m-high scarps in alluvial deposits; latest movement on the fault is older than Holocene (Menges and Pearthree, 1983; Pearthree, 1998). The Big Chino fault may have been responsible for the February 4, 1976 Chino Valley earthquake ($M_b=4.9$), analysis of which indicated normal movement along a northwest-trending fault plane dipping 40° to the southwest (Eberhart-Phillips and others, 1981).

Another large fault system, the Verde fault zone, shows evidence of Quaternary movement (Pearthree, 1998). It forms a northwest-striking zone of faults along the western margin of Verde Valley, progressively downdropping to the east. Anderson and Creasey (1958) suggested that as much as 300 m (980 ft) of offset on this fault may have occurred during the Precambrian, although this early faulting is not related to the present basin. Most of the offset took place during the late Miocene and Pliocene (Bressler and Butler, 1978; Nations and others, 1981), displacing Tertiary rocks as much as 1000 m (3280 ft; Twenter and Metzger, 1963). Evidence of Quaternary offset is limited to an 8-km-long section of fault scarps in the southern part of the fault zone, called the Camp Verde fault by Menges and Pearthree (1983).

Faults can serve as conduits or barriers to ground-water movement. On a regional scale, northwest -striking fractures throughout the Colorado Plateaus area in northern Arizona tend to be open to fluid flow (Thorstenson and Beard, 1998; L.S. Beard, oral commun., 1999).

Twenter and Metzger (1963) argue that the Verde fault zone acts as a barrier to ground-water flow and directs ground water to the southeast along its fractures and joints. Well yields in the middle Verde basin are generally improved by the presence of solution cavities along fractures in the Redwall Limestone and Martin Limestone (Owen-Joyce and Bell, 1983, p. 20). These limestone units are exposed along the margins of the Big Chino basin and the canyon walls of the upper Verde River (Fig. 2).

GRAVITY AND AEROMAGNETIC DATA

Details of the processing techniques of the high-resolution aeromagnetic data collected for the study are given in Langenheim and others (2000; 2002). Flight lines were oriented east-west, spaced 150-300 m (0.093-0.186 mi) apart, and flown at an average terrain clearance of 350 m (1,148 ft). Significant deviations from the average terrain clearance are as much as 1087 m (3,566 ft) over Verde Valley and 700 m (2,297 ft) over the area east of Granite Mountain north of Prescott (Langenheim and others, 2002). North-south control lines were spaced 3.0 km (1.83 mi) apart. Total flight distance was 27,291 km (16,958 mi). To shift anomalies over their respective sources, the magnetic data were reduced to the pole (Fig. 3; Blakely, 1996). We assume in this study that there are no significant areas with directions of remanent magnetization that are significantly different than the present Earth field direction in order to justify application of the reduction to pole transformation to the aeromagnetic data.

About 3,300 gravity stations (Frank, 1984; Smith, 1984; Water Resources Associates, 1989; National Geophysical Data Center, 1999; Langenheim and others, 2000, 2002) were used to produce an isostatic gravity anomaly map of the region (Fig. 4); 862 stations were collected as part of this study. The data were reduced using a density of 2.67 g/cm³. The isostatic gravity data reflect density variations within the middle and upper crust (Simpson and others, 1986). Details on the processing of the gravity data are given in Langenheim and others (2000; 2002). Gravity stations are non-uniformly distributed in the region. Station spacing is on average 1 station per 2 km² (0.772 mi²) although the station spacing is as low as 1 station per 10 km² (3.86 mi²) even within parts of Big Chino and Little Chino Valleys.

FILTERING TECHNIQUES

Magnetic and gravity anomalies are produced by a variety of sources of variable size and depth. Superposition of anomalies from multiple sources can result in interpretational ambiguities. For example, both Proterozoic crystalline and Tertiary volcanic rock types have magnetic units, but may be characterized by anomalies of differing wavelengths (or characteristic length). Shallow sources typically cause short-wavelength anomalies, whereas deep sources cause long-wavelength anomalies. Generally, the Tertiary volcanic rocks, comparatively thinner and shallower than Proterozoic crystalline rock, should produce shorter-wavelength anomalies. Several analytical techniques were applied to the geophysical data to distinguish particular anomaly characteristics, such as wavelength or trend.

Wavelength Separation

To emphasize both short-wavelength anomalies caused by shallow sources (e.g. Tertiary volcanic rock) and long-wavelength anomalies (e.g. Proterozoic crystalline rock), a match filter was applied (Phillips, 2001). Match filtering separates the data into different wavelength components by modeling the observed spectra as a sum of distinct equivalent source layers at increasing depths (see Phillips, 2001). Figure 5 shows the resulting separated fields produced

by the dipole equivalent-source layers at 0.76, 2.93, and 12.24 km depths, associated with increasingly deeper sources. Another method, the first vertical derivative of the magnetic data (Fig. 6) suppresses longer-wavelength trends caused by more deeply buried magnetic rock types (Blakely, 1996). A third method to sharpen the effects of near-surface sources involves analytically upward continuing the magnetic or gravity field by a small interval (100 m for the magnetic data, Fig. 7; 1 km for the gravity data because of the non-uniform distribution of gravity stations, Fig. 8) to generate a regional or smoothed field. Upward continuation is the transformation of magnetic or gravity data measured on one surface to those that would be measured on a higher surface (farther from the source); this operation tends to smooth the data by attenuation of short-wavelength anomalies (Dobrin and Savit, 1988). This smoothed, upward continued field is then subtracted from the unfiltered field to produce a residual field. The unfiltered and residual fields (Figs. 3, 5, 6, and 7 for the magnetic field, Figs. 4 and 8 for the gravity field) illustrate the effectiveness of this approach to highlight subtle geologic features. To emphasize the smoothing effect of thick basin fill or the significant deviation from the average terrain clearance in Verde Valley on the wavelength of observed magnetic anomalies, the data were upward continued 750 m, which was the maximum deviation from the average terrain clearance. Comparing this smoothed map to the reduced to pole magnetic map (Fig. 9) shows that short-wavelength anomalies are greatly attenuated and illustrates the effectiveness of wavelength separation to determine the depths of magnetic sources.

Geophysical Boundaries

To help delineate structural trends and gradients expressed in the gravity field, a computer algorithm was used to locate the maximum horizontal gravity gradient (Cordell and Grauch, 1985; Blakely and Simpson, 1986). Concealed basin faults in Verde and Williamson Valleys were mapped using horizontal gradients in the gravity field (dashed red lines on Fig. 2). Gradient maxima occur approximately over steeply-dipping contacts that separate rocks of contrasting densities. For moderate to steep dips (45° to vertical), the horizontal displacement of a gradient maximum from the top edge of an offset horizontal layer is always less than, or equal to, the depth to the top of the source (Grauch and Cordell, 1987). Magnetization boundaries (Fig. 10) were calculated in a similar way as described in Blakely and Simpson (1986), using the magnetic potential field produced from the residual magnetic field shown in Figure 7. Concealed basin faults in Lonesome Valley and the upper Agua Fria basin were mapped using a combination of the magnetic boundaries and well data.

PHYSICAL PROPERTIES

Magnetic and gravity data reflect the surface and subsurface distribution of magnetization and density. The magnetization (emu/cm^3) of a rock is the sum of remanent and induced components. The remanent component is not easily measured in the field and will be discussed later. The induced component depends on magnetic susceptibility (cgs unit), which is easily measured in the field. Magnetic susceptibility and density information of exposed rock types is critical to determining the sources of gravity and magnetic anomalies. Table 1 summarizes the magnetic susceptibility and density data of various rock types collected for this study.

The most magnetic rock types in the study area, in general, are Tertiary volcanic rocks, having an average magnetic susceptibility of 0.87×10^{-3} cgs units. The latite-andesites are generally slightly less magnetic than the basalts, although they exhibit a wider range in magnetic properties, ranging from 0.04×10^{-3} cgs units for oxidized latite-andesites to 5.04×10^{-3} cgs units

for a Tertiary hornblende-bearing latite. The most magnetic Tertiary basalt sample is a magnetite-rich basalt, tentatively assigned to the Hickey Basalt (4.0×10^{-3} cgs units).

Proterozoic rocks, although slightly less magnetic in general than the Tertiary volcanic rocks, include the highest magnetic susceptibility readings (6.37×10^{-3} cgs units) for the study area. These rocks are very heterogeneous, as indicated by standard deviations that exceed the average susceptibility values for the four main rock types. In general, the metasedimentary rocks are not magnetic, except for an iron-rich metachert that forms a minor lithologic constituent exposed south of the towns of Prescott and Prescott Valley (Krieger, 1965) and metagraywacke exposed on the western side of Sullivan Buttes. Metavolcanic rocks, gabbros and some of the intrusive rocks can be quite magnetic and therefore can produce prominent magnetic anomalies. Granodiorites and granites show a wide range in susceptibility, although individual granodiorite and granite plutons may be characterized by narrower ranges in susceptibility. For example, the Prescott granodiorite, exposed near Prescott, has a range of 0.04 to 1.27×10^{-3} cgs units for 8 samples (mean of 0.81). The Minnehaha Granodiorite, exposed in the southern Bradshaw Mountains, on the other hand, is less magnetic, showing a range in susceptibility of 0.0008 to 0.028×10^{-3} cgs units for 5 samples (mean of 0.004).

Limited physical property data for Tertiary sedimentary rocks (21 samples) suggest that these rocks can produce measurable magnetic anomalies, although their average susceptibility is 0.15×10^{-3} cgs units, which is considerably less than those of the Tertiary volcanic and Proterozoic rocks. Detritus from the volcanic rocks probably is responsible for the magnetic properties of the Tertiary sedimentary rocks. The most magnetic Tertiary sedimentary samples were volcanoclastic rocks immediately beneath Tertiary basalt (?) sampled at depths of 740-766 ft (226-233 m) in WV-3 in Williamson Valley (Fig. 1).

The magnetic properties of the Paleozoic sedimentary rocks (Table 1) are very weak, resulting in low-amplitude magnetic anomalies generally undetectable by airborne surveys.

Magnetic susceptibility contributes to one component of the total magnetization of a rock. The other component, the remanent magnetization, is a function of the direction of the Earth's magnetic field when the rock acquired its magnetization. Remanent magnetization can be an important component of the magnetization of the Tertiary volcanic rocks, but is unlikely to contribute to the magnetization of the other magnetic rock types in the study area because of the great age and coarse grain size of the Proterozoic rocks. Remanent magnetization could be significant for Cretaceous plutonic rocks, as shown for Mesozoic plutonic rocks elsewhere in Arizona (Gettings, 2002); in the study area these rocks do not cause significant anomalies (Fig. 10). The Tertiary basalts in this region typically include lava flows that individually may have a uniform direction of magnetization. The basalts are of normal or reversed polarity, as indicated by the magnetostratigraphic study by McKee and Elston (1980) in the Verde Valley area. Two basalt flows exposed near Sullivan Lake in and near the Verde River canyon were collected for paleomagnetic measurements and found to have reversed directions, confirming interpretations of short-wavelength, negative anomalies there (Langenheim and others, 2005). Natural remanent magnetizations were high, ranging from 10^{-3} to 10^{-1} emu/cm³, yielding Koenisberger ratios (Q, the ratio of remanent to induced magnetization) of 1.25 to 400. The magnetic remanence of two latite-andesites exposed in the Sullivan Buttes area was also measured, indicating reversed directions (declinations (D) of 149° and 182° and inclination (I) of -47° and -58° ; the present-day direction of $D=13^{\circ}$ and $I=61^{\circ}$) and the intensity of the remanent magnetization is about $1-3 \times 10^{-3}$ emu/cm³. This information supports the

interpretation that many of the circular magnetic lows in Figures 3, 5, 6 and 7 may be caused by reversely magnetized lati-andesite plugs.

The density measurements for this study (Table 1) are consistent with earlier data (Cunio, 1985; Frank, 1984; Langenheim and others, 2005). Proterozoic rocks are dense (average value of 2.76 g/cm^3), but exhibit a wide range in values. For instance, gabbro and metavolcanic rocks can be as dense as 3.09 and 3.15 g/cm^3 respectively; however, representative density values of aplites and pegmatites are lower (2.59 g/cm^3). The metasedimentary and granitic rocks are characterized by densities intermediate to these values. The density of the Paleozoic rocks is indistinguishable from those of the Proterozoic granitic rocks, although the carbonate formations (Martin Formation and Redwall Limestone, 2.72 g/cm^3) are denser than the clastic formations (Tapeats Sandstone, Hermit Shale, or Supai Group rocks; 2.53 g/cm^3). Similarly, the Tertiary basalts may be difficult to distinguish from the pre-Cenozoic rocks, with an average density of 2.69 g/cm^3 . The lati-andesites are less dense (average 2.55 g/cm^3), although densities of vesicular basalts and some of the lati-andesites in the study area are as low (2.16 g/cm^3) as those of the Tertiary sedimentary rock samples.

Only ten direct density measurements of the Tertiary sedimentary sequence were made in the study area; these measurements are undoubtedly biased towards higher densities because of the difficulty in obtaining a hand sample in unconsolidated materials. They are significantly less dense ($\sim 2.46 \text{ g/cm}^3$) than most of the other rock types. The average density of the Verde Formation based on 21 measurements (Smith, 1984) is 2.16 g/cm^3 (dry) and 2.41 g/cm^3 (saturated) and suggests that our average density is indeed skewed toward higher values. No measurements were made on Quaternary sedimentary deposits for this study. Because of the difficulty of obtaining direct density measurements on Quaternary and Tertiary sedimentary rocks, one must rely on indirect information previously discussed at length by Langenheim and others (2005) and summarized in Figure 11. The most direct measure of the density of the sedimentary sequence comes from borehole gravity surveys outside the study area, such as those compiled for the state of Arizona (Tucci and others, 1982, *their* Figure 3) and those compiled for the Basin and Range province (Jachens and Moring, 1990).

GEOPHYSICAL ANOMALIES

The aeromagnetic data show distinctive magnetic anomaly patterns associated with distribution of Proterozoic basement and Tertiary volcanic rocks. The anomalies over Proterozoic exposures contrast with those over exposures of Tertiary volcanic rocks, which produce distinctive high-amplitude, short-wavelength magnetic anomalies. The anomalies produced by buried Tertiary volcanic rocks are particularly evident over much of Lonesome Valley and Little Chino Valley; anomalies produced by outcrops of Tertiary volcanic rocks are obvious in the Black Hills, Sullivan Buttes, and the area around Paulden. Many of the Tertiary lati-andesites coincide with very strong circular magnetic lows indicative of volcanic plugs. Tertiary basalts generally produce a “worm-like” magnetic anomaly pattern. Anomalies associated with Proterozoic rocks tend to be smoother and less noisy than their counterparts over Tertiary volcanic rocks.

The magnetic anomaly map of the area can be divided into two main sections east and west of the Black Hills. East of the Black Hills, distinctive high-amplitude, short wavelength magnetic anomalies are closely associated with exposures of Tertiary volcanic rocks (Fig. 10). This pattern contrasts with smooth, generally low magnetic values present over Verde Valley. The

subdued nature of these anomalies is probably caused by two factors: (1) the increased flight elevation (height of the magnetic sensor) above the ground surface in this region and (2) the substantial thickness of relatively non-magnetic Verde Formation in the Verde Valley. Volcanic rocks may be present throughout the subsurface in Verde Valley, but because of the attenuation of these anomalies, it is not possible to map their distribution with confidence using unfiltered aeromagnetic data. The amount of smoothing is exemplified in the area around Page Springs (Fig. 9); the magnetic signature of volcanic rocks at depths (or distances) greater than 750 m is indistinguishable from that of Proterozoic basement. Even using filtered data, as in the grayshade vertical derivative map (Fig. 6), wells that did penetrate volcanic rocks in Verde Valley coincide with only very subtle anomalies.

The dominant anomaly trend in the Verde Valley and areas east of the Black Hills is northwest, with subordinate northeast and north-northeast trends. The northwest trends are parallel to the dominant young faults mapped on the west side of the valley. North- to northeast-striking anomalies are associated with Proterozoic basement rocks. Directly west of the Black Hills is a 40-km long, linear north-striking magnetic high that extends from the town of Prescott Valley north towards Perkinsville. Its source resides within the Proterozoic basement, because the magnetic high can be traced onto scattered outcrops of Proterozoic gabbro (Fig. 10).

In the Bradshaw Mountains and Black Hills, anomalies caused by Proterozoic basement rocks typically strike north to northeast, parallel to steep foliations mapped in these rocks (DeWitt and others, in press). Intense magnetic highs coincide with exposures of gabbro and metavolcanic rocks (Fig. 10). Lower magnetic values coincide with exposures of some of the felsic plutonic rocks, such as the Prescott Granodiorite in the southwest corner of the survey area, and the Cherry Tonalite (of DeWitt and others, in press) in the Black Hills, and metasedimentary rocks such as the quartzite of the Mazatzal Group southeast of Del Rio Springs. Superposed on the low magnetic values over the felsic plutonic rocks are anomalies (amplitudes generally <100 nT) that strike north to northeast. In the Black Hills, these north- to northeast-striking anomalies over the Cherry Tonalite contrast with a northwest fabric associated with scattered exposures of gabbro and with the areas to the east in Verde Valley.

The magnetic field over the alluvial deposits of Lonesome Valley, Little Chino Valley, and upper Agua Fria basin shows many short-wavelength, northwest- and north-trending anomalies. Because alluvium is commonly weakly magnetic, many of these anomalies probably originate from volcanic rocks concealed beneath the surface and can in places be traced to outcrops such as Glassford Hill west of the town of Prescott Valley. The irregular texture of the magnetic field over these alluvial deposits contrasts with the relatively smooth magnetic character of much of Big Chino Valley, parts of Williamson Valley, and part of Little Chino Valley east of Granite Mountain. The smooth character of the magnetic field over Big Chino and Williamson Valleys can be attributed to a greater depth to magnetic basement because of thick basin fill that is at least 600 m (Langenheim and others, 2005; this study). The smooth character of magnetic anomalies in the Little Chino Valley adjacent to Granite Mountain is mostly caused by the increased height of as much as 700 m of the magnetic sensor above the ground surface in this region (Langenheim and others, 2002, *their* Fig. 4)

Extensive outcrops of the Paleozoic sedimentary sequence (thickness 0-200 m) generally produce a relatively featureless magnetic field. The first derivative map (Fig. 6) shows the generally smooth magnetic character associated with the Paleozoic sequence north of Hickey Mountain and the area around Sedona. Surprisingly, this smooth character does not coincide

with similar rocks on Big Black Mesa. Instead, large-amplitude, relatively short-wavelength magnetic highs are present over these weakly magnetic sedimentary rocks. The source of these anomalies is thus likely in the Proterozoic basement and concealed by Paleozoic units. Several small exposures of Proterozoic granitic rocks along the Big Chino fault (Krieger, 1967) are the most likely source of the Big Black Mesa aeromagnetic high. This is supported by measured magnetic susceptibilities of the Chino Valley granite as high as 2.07×10^{-3} (cgs units). The high is truncated by the Big Chino fault on its southwestern margin (Langenheim and others, 2000).

Although Paleozoic rocks near Sedona and north of Hickey Mountain are characterized by smooth anomalies, some of these anomalies have considerable amplitude. For example, the area around Sedona is part of a broad magnetic high, with an amplitude of >250 nT (Fig. 3). Oil-test wells in the Sedona area encountered Proterozoic granite beneath 300-500 m (980-1640 ft) of Paleozoic sedimentary rocks (Peirce and Scurlock, 1972). The long-wavelength nature of the anomaly suggests that the source of the anomaly is buried deeper than 300-500 m (980-1640 ft); see, for example, the prominent magnetic highs at matched-filter depths of 2.93 and 12.24 km in the Sedona area (Fig. 5). This area also coincides with a large positive gravity anomaly (Fig. 4), suggesting a more mafic rock type of Proterozoic age may be the source of both the gravity and long-wavelength magnetic positive anomalies.

The gravity field is dominated by gravity highs along the northeastern part of the study area, with lower gravity values in the southwestern part of the study area (Fig. 4). Superposed on this regional field are local gravity lows in the valley areas. Big Chino Valley is characterized by a gravity low, bounded on the northeast by the Big Chino Fault. The deepest part of the basin, as suggested by the lowest gravity values within the valley, is near Bureau of Reclamation drillhole CV-DH3. The Big Chino gravity low narrows to the northwest and becomes less prominent. To the southeast, gravity values increase towards Sullivan Lake, corresponding with shallower basin deposits and Proterozoic outcrops east of Sullivan Lake.

Little Chino Valley is characterized by higher gravity values than those over Big Chino Valley, suggesting that the basin fill beneath Little Chino Valley is less than 1 km (3280 ft; Langenheim and others, 2000). South of the town of Chino Valley is an east-west striking gravity gradient, that is bordered by a large gravity low to the south. This low could be caused by a deep basin centered near the intersection of Highway 89 and alternate route 89, but a more likely explanation is a thick stock of Prescott Granodiorite (Cunion, 1985). The gravity low extends over Proterozoic Prescott Granodiorite and Dells Granite. These rocks are less dense (averages of 2.67 and 2.61 g/cm³, respectively) than the some of the more mafic metavolcanic rocks and gabbro within Proterozoic basement (2.81 and 2.93 g/cm³ for metavolcanic and mafic igneous rocks, Table 1). This low may mask more subtle gravity lows caused by locally thick (as much as 200-300 m) accumulations of basin fill. Local gravity lows highlighted in the residual gravity map (Fig. 8) may reflect these local sub-basins.

A northwest-trending gravity low over Williamson Valley may reflect a relatively deep (1-2 km) sedimentary basin or a low-density pluton (Langenheim and others, 2000) or a combination of the two. The gravity low also coincides with relatively low magnetic values (Fig. 4), especially for the shallow matched-filter depth (Fig. 5), and a relatively smooth magnetic field (Fig. 6, 7). The basin interpretation is preferred here because the gravity low does not extend across Proterozoic outcrops exposed to the east of the gravity low. A drillhole completed for the city of Prescott, WV-1, supports the basin interpretation; the drillhole

penetrated 460 m (1500 ft) of Tertiary clastic fill without encountering Proterozoic basement rocks (T. Merrifield, oral commun., 2002; Figs. 4, 8).

Like Williamson Valley, Verde Valley is characterized by a series of northwest-trending gravity lows. The lows, approximately 35 km (22 mi) long and 8-10 km (5-6 mi) wide, lie within the southwestern half of the valley. The western margin of the Verde Valley gravity lows is nearly coincident with the central and southern parts of the Verde fault zone south of a point 4 km (2.5 mi) north of the old Cherry road. The western margin of the gravity lows lies 1-2 km (0.6-1.2 mi) east of the mapped trace of the northern part of the fault zone. The very linear northeastern margin of the gravity lows also has a northwest trend, suggestive of a fault origin. Near the intersection of I-17 and Hwy 260, the eastern edge of the gravity low changes to a more southerly strike for a distance of about 10 km (6.2 mi), before reverting to a southeasterly strike south of Camp Verde. The lowest gravity values are northwest of the change in strike of the eastern margin. A smaller gravity low, about 8 km (5 mi) long, lies to the south of the step and is enhanced in the filtered version of the gravity field (Fig. 8). The southern extent of this gravity low, outside the boundary of the new aeromagnetic data, is poorly defined by gravity data. Another gravity low, located about 10 km (6 mi) west of Camp Verde, is on the footwall side of the Verde fault. The low could reflect a basin concealed beneath Tertiary basalt flows or lower-density Proterozoic basement rocks. Because the gravity field is affected both by changes in thickness of the Cenozoic deposits and density variations in the underlying Paleozoic and Proterozoic rocks, a method described below attempts to separate these two sources.

DEPTH TO BASEMENT

Method

In this section, depth to bedrock, here defined to be rocks of pre-Cenozoic age, is calculated beneath the study area in order to define the shape of the basins beneath valleys within the study area and to determine the geometry of bounding and internal faults.

The method used in this study to estimate the thickness of Cenozoic rocks (rocks above bedrock) is a modified version of an iterative method developed by Jachens and Moring (1990) that incorporates drill hole and other geophysical data (Fig. 12). The inversion procedure allows the density of bedrock to vary horizontally as needed, whereas the density of basin-filling deposits is specified by a pre-determined density-depth relationship. Two density-depth functions listed in Table 2 were used to provide two end-member models. In this iterative approach, a first approximation of the bedrock gravity field is derived from gravity measurements made on exposed pre-Cenozoic rocks or bedrock, augmented by appropriate bedrock gravity values calculated at sites where depth to bedrock is known. This approximation, which ignores the gravity effects of nearby basins, is subtracted from the observed gravity, which provides the first approximation of the basin gravity field. Repeating the process using the specified density-depth relation, the thickness of the basin-fill deposits is calculated. The gravitational effect of this first approximation of the basin-fill layer is computed at each known bedrock station. This effect is, in turn, subtracted from the first approximation of the bedrock gravity field and the process is repeated until successive iterations produce no substantial changes in the bedrock gravity field.

The inversion presented here does not take into account lateral variations in the density distribution of the Cenozoic deposits, which may be an important source of error in this region,

particularly in areas underlain by thick, dense basalt flows or complex, intertonguing of Cenozoic rocks of differing densities. Because of the wide density range of the local Cenozoic volcanic rocks and their limited thickness (basalts are generally less than 100 m thick), the same density-depth relationship was assumed for Cenozoic volcanic rocks as for the Cenozoic sedimentary deposits. One might consider including the basalts with the pre-Cenozoic bedrock. However, the difficulty of distinguishing dense basalt from lower-density latite-andesite or vesicular basalt in driller's logs and the presence of gravels beneath and interbedded with both the basalts and latite-andesites made this approach intractable.

The inversion method has been shown to be effective in determining the general configuration of the pre-Cenozoic bedrock surface in Nevada (Phelps and others, 1999). They showed that the model bedrock surface of Yucca Flat (Nevada Test Site, northwest of Las Vegas, Nevada) was a reasonable approximation of the true surface based on comparison of calculated basin depths with densely-spaced drill hole data. The general shape of the basin did not change significantly with additional well control. Furthermore, it appears that lateral variations in basin density, unless abrupt, do not change the overall modeled general shape of the basin. Although the method is a good tool at predicting the shapes of basins, it can be less effective in estimating the magnitude of basin thickness, especially in basins having thick basalt flows or in areas of poor well control. Below is a discussion of the sources of error in the depth to basement calculations.

Estimating Uncertainties in Basin Depth

Two basin models (Fig. 13) were created using two different density-depth functions (Table 2). Figure 13a shows the basin model using the density-depth function based on the Basin and Range density-depth function of Jachens and Moring (1990); Figure 13b is the basin model using the density-depth function based on borehole measurements in Arizona (Tucci and others, 1982). Both models use the same bedrock gravity values and well control and thus the shapes of the basins are similar, differing only in the magnitude of the predicted basin thickness. The inversion using the Basin and Range density-depth function is preferred because of the lack of geologic evidence around the margins of the basins for greater basin fill thickness predicted by the Tucci inversion and because of the consistent overestimation of basin fill thickness at wells that did penetrate basement in Big Chino and Williamson Valleys (Langenheim and others, 2005). Figure 14 shows the bedrock gravity from the inversion using the Basin and Range density-depth function.

The gravity anomaly values used in the inversion are relative to the reduction density of 2.67 g/cm^3 . If the topography consists of rocks that differ from the reduction density, errors in the basin fill thickness can be introduced. If we recalculate basin fill thickness using gravity data reduced to a higher reduction density (2.76 g/cm^3 , the average Proterozoic density), the error from this source of uncertainty is less than 100 m, except for the Verde Valley where the error is as high as 150 m (500 ft).

The inclusion of wells that intersected bedrock greatly improves the fit of the predicted basin fill thickness to the actual thickness found at these wells (Fig. 13c). The basin thickness predicted by the inversion, where constrained by well data, is within 50 m (160 ft) of the real thickness at these points (average is 1 m or 3 ft), thus providing a sense of the maximum error where the model is well constrained. Without wells used as constraints, the average misfit is 16 m (52 ft), with the total basin thickness at one well as much as 1.1 km (3,600 ft) less than that predicted by the inversion. This well was in the middle of Big Chino Valley and illustrates

the importance of having independent control near the center of the basin. Estimation of the absolute magnitude of basin thickness in areally large basins is hampered because most of the wells that reach bedrock are fairly close to bedrock outcrops. No deep wells in the center of Verde Valley penetrate bedrock.

Another way to validate the models is to compare the predicted basin thickness with the minimum thickness of Cenozoic deposits found in wells that did not bottom in pre-Cenozoic rock. In most of the study area, the basin thickness predicted by the models is generally greater than that found in these wells (Fig. 15; purple areas are where model thickness is supported by these wells). Misfits at only a few wells are more than the maximum error (50 m or 160 ft) for the well constrained inversion. Most of the large misfits (labeled “g” on Fig. 15) coincide with large gravity gradients. If the basin thickness is changing abruptly, the inversion may not be capable of resolving the actual thickness within the grid interval (300 m or 980 ft); this is a likely explanation for the misfits in Big Chino and Verde Valleys. For Little Chino Valley, the largest misfit coincides with not only a large gravity gradient, but also a large positive gravity anomaly in the western part of the valley (Figs. 4 and 15). Without well control to constrain the bedrock gravity, the modeling process will not show a basin in the vicinity of the gravity high. For Verde Valley, the absence of wells penetrating bedrock near the center of valley adds even more uncertainty to the basin depth results because of the uncertainty in the bedrock gravity field. Another source of uncertainty for Verde Valley is potentially thick volcanic flows in the downdropped block of the Verde fault zone, adjacent to the western margin of Verde Valley. For example, Hickey basalt is as much as 400 m (1,300 ft) thick on the upthrown block in the Black Hills.

Depth to Basement Results

Big Chino Valley

The results presented here build upon, and extend farther north of, those of Langenheim and others (2005). The incorporation of the CVR wells as constraints for the inversion confirms that the pre-Cenozoic bedrock gravity beneath Big Chino Valley is relatively featureless (Fig. 14), as inferred by Langenheim and others (2005). The lack of significant bedrock gravity variations suggests that there may be similar basement rock types beneath Big Chino Valley and Big Black Mesa. The aeromagnetic data suggest that the magnetic basement beneath Big Black Mesa does extend southwest of the Big Chino fault (Figs. 3 and 5), at least as far southeast as the scarp near the intersection of Big Chino Wash and Pine Creek (BCw-PC on Fig. 2). Large changes in bedrock density are not anticipated beneath the eastern part of Big Chino Valley, suggesting that at least the shape of the basin inferred from the gravity inversion should not change significantly with additional data.

A narrow (3-4 km), deep basin underlies the northeastern part of Big Chino Valley, which extends approximately 20 km (12.4 mi) northwest of drillhole CV DH-1 (Fig. 13). The northeastern margin of the basin is steep and well-defined by the Big Chino fault. The southwestern boundary of the basin is less well defined, partly because of the relative paucity of gravity measurements. The southwestern boundary appears to be less steep and is most likely formed by a number of faults, none mapped at the surface. One set of inferred faults parallels and is 3-4 km (1.9-2.5 mi) southwest of the Big Chino fault (as suggested by Ostenaar and others, 1993). Another set of faults farther west strikes more northerly and parallels the gravity gradient marking the western edge of the gravity low (Fig. 4). The northern margin of the deep basin is at the intersection of these inferred northerly-striking western margin faults

with the Big Chino fault. South of, and aligned with a marked change in strike in the Big Chino fault is a bedrock ridge (BR, Fig. 13) that separates the deep basin to the southeast with a shallower, wider basin to the northwest. The southern margin of the deep basin may also be fault-bounded by multiple concealed faults that parallel the scarp near Big Chino Wash (BCW-PC on Fig. 2). Decreasing basin thickness at the southeast margin of the basin corresponds to a decrease in displacement on the Big Chino fault, which terminates in a series of horsetail splays north of Paulden (Krieger, 1965).

The lateral extent of fine-grained sediments in Big Chino Valley, as delineated by water well logs (Schwab, 1995) coincides well with the outline of the gravity low (Langenheim and others, 2005). The fine-grained carbonate sediments were apparently deposited in a lacustrine or playa environment, related to interior drainage in Big Chino Valley that was attributed to damming of the valley 4-6 Ma basalt flows east of Paulden (Ostenaa and others, 1993). The presence of fine-grained material throughout the depth interval in CV-DH-3 (Fig. 1) suggests that deposition of this material predates eruption of the basalts. The lacustrine environment of the deposits may have been facilitated by downwarping of the basin by the Big Chino fault during the late Tertiary and Quaternary (Menges and Pearthree, 1983; Ostenaa and others, 1993; DeWitt and others, 2005). The bedrock ridge along the northwestern margin of the deep basin may have isolated these deposits from those in the shallower, broader basin to the northwest.

Verde Valley

The basin defined by the gravity inversion for Verde Valley is probably not as good as that for Big Chino Valley because of large variations in bedrock gravity observed around the edges of Verde Valley (Fig. 14). These bedrock gravity variations must be extrapolated across an area of basin deposits as large as 25 by 50 km without any independent well control on the depth to bedrock. To help constrain the bedrock gravity, aeromagnetic data filtered to enhance sources within the bedrock were compared to the gravity field. A strong gravity gradient along the course of the Verde River correlates with the edge of a magnetic block ("a" on Fig. 5c), suggesting that dense, magnetic basement is present beneath much of the eastern part of Verde Valley. Accordingly, several inferred bedrock gravity values in this area were added to the inversion.

The low bedrock gravity values west of the Verde fault zone at the latitude of Camp Verde are the result of low gravity values measured on the Cherry Tonalite (of DeWitt and others, in press), part of the bedrock in the southern Black Hills (Fig. 14). These values are as much as 16 mGal lower than bedrock values measured on Proterozoic metavolcanic and gabbroic rocks in the Black Hills. The average density of the Cherry Tonalite (of DeWitt and others, in press) is 2.72 g/cm^3 , which provides a density contrast of 0.10 g/cm^3 relative to the average density of Proterozoic metavolcanic rocks (Table 1) and would suggest that Cherry Tonalite (of DeWitt and others, in press) is about 10 km thick. If the density of the Cherry Tonalite (of DeWitt and others, in press) is less, as suggested by numerous felsic dikes in this area, the tonalite would be thinner. Another potential source for the low gravity values beneath Verde Valley south and east of Cherry is Cretaceous granodiorite, which has an average density of 2.67 g/cm^3 . Boulders of granodiorite within the sedimentary rocks at the base of the Hickey Formation exposed along the Verde fault may be compatible with a buried stock (DeWitt and others, in press). The buried stock would extend toward I-17, the area of the low bedrock gravity values (Fig. 14). Despite the lack of direct well information to constrain the bedrock

gravity, the combination of geologic inference and aeromagnetic data helps constrain some of the regional bedrock gravity variations beneath the valley.

The basin configuration beneath Verde Valley is complex (Fig. 13). West of the Verde River is a northwest-trending alignment of subbasins, whose western margins are the Verde fault zone (Fig. 13). East of the Verde River are relatively gentle undulations of the bedrock surface. A deep basin predicted by both inversions lies northwest of Page Springs and extends east beneath Hickey basalt. The inversion most likely overestimates the magnitude of the basin fill thickness in that area because the maximum thickness of basal sedimentary rocks in the Hickey Formation is about 50 m (DeWitt and others, in press). An alternate explanation could be lower-density Proterozoic rocks in the bedrock. With the data available, it is not possible to rule out either explanation.

The basins west of the Verde River are segmented by transverse structures. One transverse structure coincides with a 4-km left step in the trace of the Verde fault zone approximately 10 km (6 mi) northwest of Camp Verde (Fig. 13). North of the step, the western margin of the basin deviates from the mapped trace of the Verde fault zone for 12 km (7.5 mi), until it rejoins the mapped fault trace near Cottonwood. Another transverse structure is located near the southern outskirts of Camp Verde. Here the transverse structure coincides with a 3-4-km northwest or right step in the eastern margin of the basins. The step is aligned with a more northerly strike in the Verde fault zone. Both of the extreme northwestern and southeastern terminations of the basins west of the Verde River are gradual, mimicking the myriad splays of the fault zone at the southeastern terminus of the basin and decreasing displacement of the Verde fault zone at the northwestern terminus.

Verde and Big Chino Valleys are both relatively large, elongate valleys underlain by locally deep basins formed by prominent late Tertiary normal faults. Both valleys contain sedimentary deposits that formed in a lacustrine or playa environment. Tertiary volcanic rocks presumably dammed both valleys at their southern margins, contributing to lacustrine environments. The basin configuration beneath these valleys contrasts with that beneath Little Chino, Lonesome, and Williamson Valleys and upper part of Agua Fria basin discussed below.

Little Chino and Lonesome Valleys, including upper Agua Fria basin

Although the inversion results are hindered by large bedrock variations (in particular the large gravity low associated with the Dells Granite and Prescott Granodiorite), Little Chino and Lonesome Valleys have more deep wells that constrain the bedrock gravity (particularly in Lonesome Valley) than Verde Valley. The bedrock gravity (Fig. 14) shows a strong north-south gradient along the eastern margin of the valleys, consistent with the strong north-south magnetic grain shown in the aeromagnetic data filtered for deeper sources (Fig. 5b, c).

Basin inversion results for the Little Chino and Lonesome Valleys show no major, northwest-striking, deep basins. This result is not surprising, given the absence of prominent young normal faults in the valley and that known faults have less than 200 m (660 ft) of displacement (DeWitt and others, in press). The basin configuration beneath these valleys is irregular compared to that of Big Chino and Verde Valleys. In general, thicker basin fill of inferred late Miocene age is located along the northern margin of Little Chino Valley and basin fill of middle to late Miocene age is present in the upper Agua Fria basin. These pockets of thicker sediment are elongated in two major directions: north and northwest. Those basins elongated

in a north direction may be deeper according to the gravity inversion than their true depths because of north-south bedrock density variations, although some Tertiary faults also strike north. Northwest elongation of basins suggests some structural control on the basin configuration beneath these valleys because the regional strike of major late Tertiary normal faults is northwest.

Williamson Valley

Williamson Valley contains few deep wells that provide control for the gravity inversion, like its neighbor, Lonesome Valley, to the east. The combination of a gravity and magnetic low, however, that interrupts the north-striking magnetic grain of this valley suggests that the deep, northwest-striking basin in Williamson Valley is not an artifact of bedrock gravity variations. The deep basin interpretation is further supported by a well that did not penetrate bedrock at a depth of 460 m (WV-1, Fig. 1) in the center of the gravity low.

The presence of this basin is surprising given the absence of any prominent late Tertiary normal faults which suggests that it may have formed earlier, in middle to late Miocene time, than the fault-defined basins beneath Big Chino and Verde Valleys. The sediments found in both Williamson Valley drill holes include coarse-grained clastic to conglomeratic sediments deposited in an energetic environment. This suggests that the shallow bedrock ridge north of WV-3 (Fig. 13) marks the boundary between the lacustrine environment of Big Chino Valley and the coarser-grained, alluvial and fluvial deposits of Williamson Valley.

DISTRIBUTION OF VOLCANIC ROCKS IN THE SUBSURFACE

As described earlier, magnetic data are effective for mapping the distribution of buried Tertiary volcanic rocks because volcanic rock produces distinctive anomaly patterns. The distribution of buried latite-andesite plugs in Little Chino Valley were mapped by Langenheim and others (2005) and correlated with exposed Tertiary latite-andesite by the semicircular, intense magnetic lows they produce. Ground magnetic data collected over one of the inferred plugs near Del Rio Springs confirms the presence of a negative magnetic anomaly (University of Arizona Field Geophysics Class, 2003). Comparing the amplitudes of the anomaly measured at two different heights predicts a depth of 260 m (Peters, 1949) to the top of the plug. Coincident electromagnetic data indicate a resistive body at this depth and is interpreted as an intrusive body or plug. Our study expands the mapping of buried plugs into Williamson Valley, Lonesome Valley, and upper Big Chino Valley. Semicircular magnetic lows in areas covered by young sedimentary deposits that are probably Tertiary latite-andesite plugs are annotated with “p” on Figure 10.

The subsurface distribution of Tertiary basalt was also mapped in southern Big Chino Valley (Langenheim and others, 2005). Exposed Tertiary basalt produces a complicated (“wormlike”) magnetic anomaly pattern. In the area east of Paulden and directly north of the upper part of the Verde River, exposed basalt produces high-frequency magnetic anomalies. These magnetic anomalies can be traced beneath sedimentary deposits as much as 10 km (6 mi) northwest of the basalt outcrops (Fig. 10). These flows were derived from eruptive centers on the Colorado Plateau, flowed over the Mogollon Rim and into Big Chino Valley and the present-day area of the upper Verde River east of Paulden from about 4 to 6 Ma (McKee and Anderson, 1971; DeWitt and others, in press). Local sources, such as a cinder cone northeast of Paulden may also have contributed flows that fed into Big Chino Valley. The new aeromagnetic data suggest that some reversely magnetized basalt may have flowed from the

northeast down paleocanyons in the area near Paulden and north of the upper part of the Verde River. A narrow (< 1 km wide), prominent magnetic low (“c1” on Fig. 7) that is parallel to and 5 km east of highway 89 can be traced onto the negative magnetic anomalies associated with exposed Tertiary basalt. Southeast of this prominent, irregular magnetic low is an area with a smooth magnetic field that suggests thin Cenozoic sedimentary deposits lying directly on the Paleozoic sedimentary sequence.

The new aeromagnetic data also delineate the extent of buried basalt flows in the northwestern end of Big Chino Valley. The pronounced magnetic low (“c2” on Fig. 7) coincides with a narrow outcrop of basalt flanked by exposures of weakly magnetic Cambrian Tapeats Sandstone in the northeast corner of Big Chino Valley (Fig. 10). The low can be traced across the Big Chino fault where the low changes strike to the south and heads into Big Chino Valley. Here the low bisects an east-striking magnetic high (Fig. 3, 7) caused by concealed Proterozoic basement and is present only along the western edge of a bedrock ridge identified by the gravity inversion. The sinuous low, well expressed in the first vertical derivative map (Fig. 6), can be traced nearly 10 km (6 mi) beneath the valley alluvial deposits. Water wells confirm the presence of at least two basalt flows at depths of 150-180 m (500-600 feet) near the magnetic low (Ostenaar and others, 1993; Arizona Department of Water Resources, 2003).

In Williamson Valley a buried volcanic center (“vc” on Fig. 7) that covers several square kilometers is delineated by very pronounced magnetic highs about 1 km (0.6 mi) south of drillhole WV-3. The steep gradients suggest that the source is not deeply buried. This volcanic center produces an anomaly pattern different from that of the lati-andesite plugs in that the anomaly is compound, lobate, and positive (Fig. 7, 10) rather than singular, semicircular, and negative. A possible source for the magnetic anomalies was probably sampled by drillhole WV-3, which intersected 15 m (50 ft) of basalt at a depth of 216 m (710 ft). A likely source is either Hickey Basalt or 4-6 Ma basalt, although the complex, lobate anomaly pattern does not rule out the presence of lati-andesite.

The inferred volcanic center is one of many buried volcanic centers in northern Williamson Valley and there are several inferred buried lati-andesite plugs that extend west across Williamson Valley from Sullivan Buttes. Similar positive anomalies are located over sedimentary deposits in Lonesome Valley east of Highway 89. These anomalies bear some semblance to the positive anomalies over Glassford Hill (GH on Fig. 1) composed of Hickey Formation basalt. The anomalies buried beneath the alluvial deposits of Lonesome Valley appear to be elongated in a northwest direction, perhaps reflecting feeder dikes to the volcanic centers.

Mapping the subsurface distribution of Tertiary volcanic rocks in Verde Valley is hampered by the increased height of the magnetic sensor above the ground surface. The intense magnetic patterns associated with exposed volcanic rocks of the Hickey Formation at House Mountain, however, can be traced as far west as Cornville. In the northern part of Verde Valley about 10 km (6 mi) northwest of Cottonwood, subtle magnetic highs coincide with outcrops of 4-6 Ma basalt in the Verde River channel. These very subtle magnetic features can be traced another 5-10 km (3-6 mi) to the southwest and may reflect the subsurface distribution of Tertiary basalt in the Verde Formation. Alternatively, given the north-northeast strike of the anomalies, the source could reside in the Precambrian basement rocks. Helicopter-mounted or ground magnetic data in this area would help resolve the depth (and thus the age) of the source.

Langenheim and others (2005) argued that some of the volcanic plugs are likely resistant to ground-water flow, based on the relatively unfractured and impermeable nature of intrusive centers compared to the fractures and permeable nature of the flows and aprons of ejected material. A concentration of these plugs is down-gradient from Del Rio Springs in Little Chino Valley. A similar explanation may apply to the spring southeast of WV-3 in Williamson Wash, which is up-gradient from the concentration of buried volcanic centers in northern Williamson Valley.

FAULTS AND FRACTURES

Abrupt, linear changes in magnetization and density are often the result of faulting or fracturing. Because of this, linear magnetic and gravity boundaries can be used to estimate the distribution of faults and/or large fracture systems. One of the most prominent magnetic and density boundaries in the region coincides with one of the most prominent faults in the area, the Big Chino Fault. The near-colocation of the mapped fault with the magnetic and density boundaries indicates that the Big Chino Fault is steeply dipping. Other prominent magnetic and density boundaries coincide, in part, with mapped faults, that locally may project onto areas that are covered by surficial deposits. Because of this relationship, the geophysical boundaries can be used to map extensions of the faults, such as the Verde fault zone northwest of Interstate 17, beneath young sedimentary deposits. Other gravity and magnetic lineaments do not coincide with mapped faults, but can be used to infer the locations of concealed faults, such as the basin-bounding faults beneath Williamson Valley and faults forming the eastern margin of the basins along the Verde fault zone or lithologic contacts.

Below we discuss magnetic and gravity lineaments that may map potential faults and fractures that influence groundwater pathways in the area. West and northwest of exposed 4-6 Ma basalt in the Paulden area are northwest-striking anomalies that are most likely caused by relief on the upper surface of the buried basalt related to faulting or relief on the bottom surface in fault-controlled paleochannels. Mapped faults in Little Chino Valley cut across many magnetic boundaries, suggesting that their displacements are small. We include the interpreted lineaments from an earlier study (Langenheim and others, 2005) and expand the area of analysis to include the new aeromagnetic survey. Many of the lineaments are produced by physical property variations in the Proterozoic basement that parallel faults and folds mapped in outcrop. The structural grain may serve as a proxy for fracturing, an important source of permeability in these generally impermeable basement rocks. In some cases, the Precambrian structural grain may have influenced subsequent faulting.

The Bear Wallow Canyon fault, an east-west striking fault that bisects Sedona, offsets Permian sedimentary rocks. The maximum displacement is 52 m (170 ft) with offset down to the south (Levings, 1980, p. 7). A change in magnetic signature coincides with the fault, suggesting that Precambrian basement rocks are a controlling factor. The magnetic data can be used to extend the Bear Wallow Canyon fault west of its mapped extent into the northern part of Verde Valley, where it curves to the southwest. This fault appears to disrupt the regional groundwater flow (Owen Joyce and Bell, 1983, p. 18). The Cathedral Rock fault, a northwest-striking fault that merges into the Bear Wallow Canyon fault, coincides with the edge of a magnetic block (Fig. 5b, c), where it offsets weakly magnetic sedimentary rocks as much as 244 m (800 ft, Twenter and Metzger, 1963).

South of the Bear Wallow Canyon fault are pronounced northwest-striking magnetic gradients (Figs. 3 and 7). One of these gradients coincides with the trace of the Sheephead fault

(DeWitt and others, in press). The Sheepshead fault served as a growth fault during deposition of the Hickey Formation and older sediment of the Verde Formation, but not the beds at the ground surface. The aeromagnetic data can be used to project the concealed trace of this normal fault beneath the Verde Formation 5 km (3 mi) southward of its mapped location (Fig. 10). Parallel and northeast of the Sheepshead fault is another magnetic lineament. Part of this lineament coincides with a normal fault mapped through Page Springs (DeWitt and others, in press), suggesting that structure plays a role in the location of this large spring. The magnetic data can be used to project this structure another 5-10 km (3-6 mi) northwest and southeast of its mapped trace.

Prominent in the eastern part of Verde Valley are northeast-striking magnetic anomalies (Fig. 3). Some of these anomalies have gentle to moderate gradients that indicate sources within the Proterozoic basement. One such anomaly is in the northern part of the Valley near Sedona (Figs. 3 and 5c). Three narrow anomalies with steep gradients occur between Dry Beaver Creek and Lake Montezuma (Fig. 7). The width and steep gradients of these anomalies suggest that the sources are either exposed or shallowly buried. Modeling of the southernmost anomaly near Montezuma Well indicates that a source at 300 m depth (approximately the top of Proterozoic basement) would have to be no more than 1 meter wide and have unreasonably high magnetizations (1 emu/cc) to reproduce the width and amplitude of the observed anomaly. The southernmost anomaly projects northeast towards outcrops of Paleozoic sedimentary rocks, but does not continue onto these outcrops. It corresponds with outcrops of the 4-6 Ma “ramp” basalts that are considered to be the likely source. The linear nature of the anomalies suggests either fault-controlled channels or dikes. Both of these geologic scenarios have drawbacks. The 4-6 Ma basalts do not appear to fill paleochannels into the Verde Formation and dikes are not likely because virtually all of the dikes feeding Tertiary basalt flows in this area strike northwest, perpendicular to the direction of Basin and Range extension. Tertiary dikes, however, may have been influenced by the preexisting Proterozoic structural grain, as imaged by northeast-striking anomalies in the basement gravity and filtered magnetic data (Figs. 5b,c, and 14).

North of Clarkdale a north-northeast to north-northwest striking magnetic grain is pervasive (Figs. 3 and 7). The anomalies that cause this grain coincide in part with mapped faults that offset the Paleozoic sedimentary sequence and based on depth estimates based on the anomaly gradients, are caused by magnetization variations in the Proterozoic basement. Superposed on these anomalies are very subtle features that appear on the residual and vertical derivative maps (Figs. 6 and 7). The gradients and amplitudes of these anomalies suggest that weakly magnetic Paleozoic rocks are the cause.

Despite difficulties in attributing the source of magnetic and gravity lineaments to rock type and age, these data are effective in mapping structure concealed beneath sedimentary cover. Inferred major lineaments are shown on Figure 10. The relationship of groundwater flow and these lineaments, if any, may be determined by acquiring additional data, such as hydrologic data from existing and new wells.

CONCLUSIONS AND RECOMMENDATIONS

The aeromagnetic and gravity data provide new insights on the distribution of and structures associated with Tertiary volcanic rock and Proterozoic basement buried beneath younger sedimentary rocks and sediment in the upper and middle Verde River watershed. Some interpreted geologic structures may act as potential pathways or barriers for groundwater

movement. Of particular interest are the shallowly concealed latite-andesite plugs in Williamson, southern Big Chino, and northern Little Chino Valleys, manifested in the aeromagnetic data as semi-circular magnetic lows. The magnetic and limited well and resistivity data indicate that these plugs lie as much as 200-300 m (660-980 ft) beneath valley fill. The plugs may be resistant to groundwater flow, based on the relatively unfractured and impermeable nature of intrusive centers, compared to the fractures and permeable nature of the flows and aprons of ejected material. Additional volcanic centers of Hickey Formation age in Williamson and Lonesome Valleys may also influence the movement of groundwater.

The gravity data provide information on thickness of basin fill in Big Chino, Verde, Lonesome, and Williamson Valleys. Abrupt changes in basin fill thickness is used to locate faults that are buried beneath the surficial deposits in Verde and Williamson Valleys. Additional constraints, such as wells that penetrate the entire basin sequence in both valleys and more detailed gravity, electric or seismic surveys would improve the basin modeling efforts and reduce uncertainty in the interpretations presented here. These wells could also test whether the structures identified here influence groundwater movement. For example, are the northwest-striking fractures inferred from geologic and geophysical data tend to be more open to fluid flow, as proposed for similarly-oriented fractures throughout the Colorado Plateaus (Thorstenson and Beard, 1998)?

ACKNOWLEDGMENTS

We would like to thank Yavapai County for financial support. We appreciate the helpful comments of reviewers Mark Gettings and Edwin McKee.

REFERENCES

- Arizona Department of Water Resources, 2000, Verde River Watershed Study: Arizona Department of Water Resources Report, 208 p, plus appendices.
- Anderson, Phillip, 1989b, Stratigraphic framework, volcanic- plutonic evolution, and vertical deformation of the Proterozoic volcanic belts of central Arizona, *in* Jenney, J.P., and Reynolds, S.J., eds., Geologic Evolution of Arizona: Arizona Geological Society Digest 17, p. 57-148.
- Anderson, C.A., and Blacet, P.M., 1972a, Precambrian geology of the northern Bradshaw Mountains, Yavapai County, Arizona: U.S. Geological Survey Bulletin 1336, 82 p.
- Anderson, C.A., and Blacet, P.M., 1972b, Geologic map of the Mount Union quadrangle, Yavapai County, Arizona: U.S. Geological Survey Geologic Quadrangle Map GQ-997, scale 1:62,500.
- Anderson, C.A., and Creasey, S.C., 1958, Geology and ore deposits of the Jerome area, Yavapai county, Arizona: U.S. Geological Survey Professional Paper 308, 185 p.
- Arizona Department of Water Resources, 2003, Arizona Registry of Wells 55 CD-ROM, updated June, 2003.
- Blakely, R.J., 1996, Potential Theory in Gravity and Magnetic Applications: Cambridge University Press, 441 p.

- Blakely, R.J., and Simpson, R.W., 1986, Approximating edges of source bodies from magnetic or gravity anomalies: *Geophysics*, v. 51, p. 1494-1498.
- Cordell, Lindrith, and Grauch, V.J.S., 1985, Mapping basement magnetization zones from aeromagnetic data in the San Juan Basin, New Mexico *in* Hinze, W.J., ed., *The Utility of Regional Gravity and Magnetic Anomaly Maps*: Society of Exploration Geophysicists, Tulsa OK, p. 181-192.
- Cunion, Edward Joseph, Jr., 1985, Analysis of gravity data from the southeastern Chino Valley, Yavapai County, Arizona: Northern Arizona University Master's thesis, 110 p.
- Bressler, S.L., and Butler, R.B., 1978, Magnetostratigraphy of the late Tertiary Verde Formation, central Arizona: *Earth and Planetary Science Letters*, v. 38, p. 319-330.
- Davis, G.H., 1978, Monocline fold pattern of the Colorado Plateau, *in* Matthews, V. III, ed., *Laramide folding associated with basement block faulting in the western United States*: Geological Society of America Memoir 151, p. 215-233.
- DeWitt, Ed, ed., 1987, Proterozoic ore deposits of the southwestern U.S.: Society of Economic Geologists Guidebook Series, v. 1, 189 p.
- DeWitt, Ed, 1989, Geochemistry and tectonic polarity of early Proterozoic (1700-1750 Ma) plutonic rocks, north-central Arizona, *in* Jenny, J.P., and Reynolds, S.J., eds., *Geologic evolution of Arizona*: Tucson, Arizona Geological Society Digest 17, p.149-163.
- DeWitt, Ed, Langenheim, V.E., and Wirt, Laurie, 2005, Geologic framework, Verde River Headwaters region, north-central Arizona *in* Wirt, Laurie, DeWitt, Ed, and Langenheim, V.E., ed., *Geologic Framework of Aquifer Units and Ground-water Flowpaths in the Verde River Headwaters*: U.S. Geological Survey Open-File Report 04-1411.
- DeWitt, Ed, Langenheim, V.E., Force, Eric, Vance, Kelly, and Lindberg, P.A., *with* a digital database by Doug Hirschberg, Guy Pinhassi, and Nancy Shock, *in* press, Geologic map of the Prescott National Forest and headwaters of the Verde River, Yavapai and Coconino Counties, Arizona: U.S. Geological Survey Miscellaneous Investigations Map I-xxxx, scale 1:100,000, two sheets.
- Dobrin, M.B., and Savit, C.H., 1988, *Introduction to Geophysical Prospecting*: McGraw-Hill Book Company, 867 p.
- Eberhart-Phillips, Donna., Richardson, R.M., Sbar, M.L., and Herrmann, R.B., 1981, Analysis of the 4 February 1976 Chino Valley, Arizona, earthquake: *Bulletin of Seismological Society of America*, v. 71, p. 787-801.
- Elston, D.P., McKee, E.H., Scott, G.R., and Gray, G.D., 1974, Miocene-Pliocene volcanism in the Hackberry Mountain area and evolution of the Verde Valley, north-central Arizona *in* *Geology of Northern Arizona, Part II—Area studies and field guides*: Geological Society of America Guidebook 27, p. 602-610.

- Elston, D.P. and Young, R.A., 1991, Cretaceous-Eocene (Laramide) landscape development and Oligocene-Pliocene drainage reorganization of Transition Zone and Colorado Plateau: *Journal of Geophysical Research*, v. 96, no. B7, p. 12,389-12,406.
- Frank, A.J., 1984, Analysis of gravity data from the Picacho Butte area, Yavapai and Coconino counties, Arizona: Northern Arizona University Master's thesis, 91 p.
- Gettings, M.E., 2002, An interpretation of the 1996 aeromagnetic data for the Santa Cruz basin, Tumacacori, Santa Rita, and Patagonia Mountains, south-central Arizona: U.S. Geological Survey Open-File Report 02-99 (<http://geopubs.wr.usgs.gov/open-file/of02-99>).
- Grauch, V.J.S., and Cordell, Lindrith, 1987, Limitations of determining density or magnetic boundaries from the horizontal gradient of gravity or pseudogravity data: *Geophysics*, v. 52, no. 1, p. 118-121.
- Holm, R.F., Ranney, W.D.R., Witke, J.H., and Lee, K.F., 1998, Miocene volcanism and geomorphology in Verde Valley, and petrology of alkaline and mildly alkaline rocks at House Mountain shield volcano, Sedona, Arizona, *in* Duebendorfer, E.M., ed., *Geologic excursions in northern and central Arizona*: Northern Arizona University, p. 1-26.
- Jachens, R.C., and Moring, B.C., Maps of the thickness of Cenozoic deposits and the isostatic residual gravity over basement for Nevada: U.S. Geological Survey Open-File Report 90-404, 15 p., 2 plates, 1990.
- Jenkins, O.P., 1923, Verde River lake beds near Clarkdale, Arizona: *American Journal of Science*, v. 5, p. 65-81.
- Krieger, M.H., 1965, Geology of the Prescott and Paulden quadrangles, Arizona: U.S. Geological Survey Professional Paper 467, 127 p.
- Krieger, M.H., 1967, Reconnaissance geologic map of the Ashfork quadrangle, Yavapai and Coconino counties, Arizona: U.S. Geological Survey Miscellaneous Geologic Investigations Map I-499, scale 1:62,500.
- Langenheim, V.E., Duval, J.S., Wirt, Laurie, and DeWitt, Ed, 2000, Preliminary report on geophysics of the Verde River headwaters region, Arizona: U.S. Geological Survey Open-File Report 00-403, 28 p. (<http://wrgis.wr.usgs.gov/open-file/of00-403>).
- Langenheim, V.E., Hoffmann, J.P., Blasch, K.W., Dewitt, Ed, and Wirt, Laurie, 2002, Preliminary report on geophysical data in Yavapai County, Arizona: U.S. Geological Survey Open-File Report 02-352, 29 p. <http://geopubs.wr.usgs.gov/open-file/of02-352>.
- Langenheim, V.E., DeWitt, Ed, and Wirt, Laurie, 2005, Geophysical framework based on analysis of aeromagnetic and gravity data, Verde River headwaters, north-central Arizona *in* Wirt, Laurie, DeWitt, Ed, and Langenheim, V.E., ed., *Geologic Framework of Aquifer Units and Ground-water Flowpaths in the Verde River Headwaters*: U.S. Geological Survey Open-File Report 04-1411.

- Lehner, R.E., 1958, Geology of the Clarkdale quadrangle, Arizona: U.S. Geological Survey Bulletin 1021-N, p. 511-592.
- Leighty, R.S., 1998, Tertiary volcanism, sedimentation, and tectonics of the central Arizona Transition Zone, *in* Duebendorfer, E.M., ed., Geologic excursions in northern and central Arizona: Northern Arizona University, p. 59-96.
- Levings, G.W., 1980, Water resources in the Sedona area, Yavapai and Coconino counties, Arizona: Arizona Water Commission Bulletin No. 11, 37 p.
- McKee, E.H., and Anderson, C.A., 1971, Age and chemistry of Tertiary volcanic rocks in north-central Arizona and relation of the rocks to the Colorado Plateaus: Geological Society of America Bulletin, v. 82, p. 2767-2782.
- McKee, E.H., and Elston, D.P., 1980, Reversal chronology from a 7.9-11.5 m.y. old volcanic sequence in central Arizona: Comparison with ocean floor polarity record: Journal of Geophysical Research, v. 85, p. 327-337.
- Menges, C.M., and Pearthree, P.A., 1983, Map of neotectonic (latest Pliocene-Quaternary) deformation in Arizona: Arizona Bureau of Geology and Mineral Technology, Open-File Report 83-22, 48 p.
- National Geophysical Data Center, 1999, Land and Marine Gravity CD-ROMS, compiled by David Dater, Dan Metzger, and Allen Hittelman, Boulder, CO.
- Nations, J.D., Hevly, R.H., Landye, J.J., and Blinn, D.W., 1981, Paleontology, paleoecology, and depositional history of the Miocene-Pliocene Verde Formation, Yavapai county, Arizona *in* Stone, Claudia and Jenney, J.P., eds., Arizona Geological Society Digest, v. 13, p. 133-150.
- Ostenaar, D.A., Schimschal, U.S., King, C.E., Wright, J.W., Furgerson, R.B., Harrel, H.C., and Throner, R.H., 1993, Big Chino Valley groundwater study: Geologic framework investigations: Bureau of Reclamation, Denver, CO, 31 p.
- Owen-Joyce, S.J., and Bell, C.K., 1983, Appraisal of water resources in the upper Verde River area, Yavapai and Coconino counties, Arizona: Arizona Department of Water Resources Bulletin 2, 219 p.
- Pearthree, P.A., 1998, Quaternary fault data and map for Arizona: Arizona Geological Survey Open-File Report 98-24, 122 p., 1 sheet, 1:750,000 scale.
- Peters, L.J., 1949, The direct approach to magnetic interpretation and its practical application: Geophysics, v. 14, p. 290-320.
- Phelps, G.A., Langenheim, V.E., and Jachens, R.C., 1999, Thickness of Cenozoic deposits of Yucca Flat inferred from gravity data, Nevada Test Site, Nevada: U.S. Geological Survey Open-File Report 99-310, 33 p.
- Phillips, J.D., 2001, Designing matched bandpass and azimuthal filters for the separation of potential-field anomalies by source region and source type: Australian Society of

- Exploration Geophysicists, 15th Geophysical Conference and Exhibition, Expanded Abstracts CD-ROM, 4 p.
- Peirce, H.W., and Scurlock, J.R., 1972, Arizona well information: Arizona Bureau of Mines Bulletin 185, 195 p.
- Reynolds, S.J., 1988, Geologic map of Arizona: Arizona Geological Survey Map 26, scale 1:1,000,000.
- Richard, S.M., and Kneale, S.M. (eds.), 1998, Geologic map of Arizona, GIS database: Arc/INFO export file (.e00) format, 2 disks, 10 p.
- Schwab, K.J., 1995, Maps showing groundwater conditions in the Big Chino Sub-Valley of the Verde River valley, Coconino and Yavapai counties, Arizona—1992: Department of Water Resources, Hydrologic Map Series Report Number 28, Phoenix, Arizona, 1 sheet.
- Shoemaker, E.M., Squires, R.L., and Abrams, M.J., 1978, Bright Angel and Mesa Butte fault systems of northern Arizona *in* Cenozoic Tectonics and Regional Geophysics of the Western Cordillera, Smith, R.B., and Eaton, G.P., eds.: Geological Society of America Memoir 152, p. 341-367.
- Simpson, R.W., Jachens, R.C., Blakely, R.J., and Saltus, R.W., 1986, A new isostatic residual gravity map of the conterminous United States with a discussion on the significance of isostatic residual anomalies: *Journal of Geophysical Research*, v. 91, p. 8348-8372.
- Smith, M.A., 1984, Analysis of gravity data from the Verde Valley, Yavapai county, Arizona: Northern Arizona University Master's thesis, 57 p.
- Thorstenson, D.J., and Beard, L.S., 1998, Geology and fracture analysis of Camp Navajo, Arizona Army National Guard, Arizona: U.S. Geological Survey Open-File Report 98-242, 42 p.
- Tucci, P., Schmoker, J.W., and Robbins, S.L., 1982, Borehole-gravity surveys in basin-fill deposits of central and southern Arizona: U.S. Geological Survey Open-File Report 82-473, 24 p.
- Twenter, F.R., and Metzger, D.G., 1963, Geology and ground water in Verde Valley—the Mogollon rim region, Arizona: U.S. Geological Survey Bulletin 1177, 132 p.
- Tyner, Grace Nell, 1984, Geology and petrogenesis of the Sullivan Buttes latite, Yavapai County, Arizona; field and geochemical evidence: Austin, University of Texas, Ph.D. dissertation, 286 p.
- University of Arizona Field Geophysics Class, 2003, Geophysical Surveys near Chino Valley, Arizona: Laboratory for Advanced Subsurface Imaging LASI-03-1, 74 p.
- Water Resources Associates, Inc., 1989, Hydrogeology investigation, Big Chino Valley, Yavapai county, Arizona, Phase I, Volumes I & II: consultants reports for City of Prescott, City Attorney's Office, Prescott, Arizona, November 29, 1989, 2 volumes.

Wilson, E.D., 1939, Precambrian Mazatzal revolution in central Arizona: Geological Society of America Bulletin, v. 50, p. 1131-1163.

Wirt, Laurie, and Hjalmarson, H.W., 2000, Sources of springs supplying base flow to the Verde River headquarters, Yavapai County, Arizona: U.S. Geological Survey Open-File Report 99-0378, online release (<http://pubs.usgs.gov/of/1999/ofr-99-0378/>), 54 p.

Table 1. Densities (g/cm³) and magnetic susceptibilities (10⁻³ cgs units) of hand samples collected for this study

<i>Tertiary sedimentary rocks</i>		Susceptibility	Average
<u>Density Range</u>	<u>Average Density</u>	<u>Range</u>	<u>Susceptibility</u>
2.16-2.67	2.49+/-0.17(N=10)	0.00-0.55	0.15+/-0.17 (N=21)
<i>Tertiary volcanic rocks</i>		Susceptibility	Average
<u>Density Range</u>	<u>Average Density</u>	<u>Range</u>	<u>Susceptibility</u>
2.16-2.98	2.69 +/-0.19 (N=103)	0.03-3.98	0.87+/-0.80 (N=105)
Tertiary basalt		Susceptibility	Average
<u>Density Range</u>	<u>Average Density</u>	<u>Range</u>	<u>Susceptibility</u>
2.16-2.98	2.73 +/-0.18 (N=79)	0.03-3.98	0.93+/-0.73 (N=81)
Tertiary latite-andesite		Susceptibility	Average
<u>Density Range</u>	<u>Average Density</u>	<u>Range</u>	<u>Susceptibility</u>
2.27-2.91	2.55+/-0.13(N=24)	0.04-5.04	0.67+/-0.97 (N=24)
<i>Paleozoic sedimentary rocks</i>		Susceptibility	Average
<u>Density Range</u>	<u>Average Density</u>	<u>Range</u>	<u>Susceptibility</u>
2.26-2.84	2.62+/-0.15(N=41)	0.00-0.02	0.00 (N=35)
Paleozoic carbonate rocks		Susceptibility	Average
<u>Density Range</u>	<u>Average Density</u>	<u>Range</u>	<u>Susceptibility</u>
2.62-2.84	2.72+/-0.07(N=19)	0.00-0.01	0.00 (N=19)
Paleozoic siliciclastic rocks		Susceptibility	Average
<u>Density Range</u>	<u>Average Density</u>	<u>Range</u>	<u>Susceptibility</u>
2.26-2.75	2.53+/-0.13(N=22)	0.00-0.02	0.00 (N=22)
<i>Proterozoic rocks</i>		Susceptibility	Average
<u>Density Range</u>	<u>Average Density</u>	<u>Range</u>	<u>Susceptibility</u>
2.59-3.15	2.76+/-0.13(N=116)	0.00-6.37	0.73+/-1.22 (N=240)
Proterozoic metavolcanics		Susceptibility	Average
<u>Density Range</u>	<u>Average Density</u>	<u>Range</u>	<u>Susceptibility</u>
2.63-3.09	2.82+/-0.13(N=30)	0.00-6.37	0.55+/- 1.20 (N=78)
Proterozoic metasedimentary		Susceptibility	Average
<u>Density Range</u>	<u>Average Density</u>	<u>Range</u>	<u>Susceptibility</u>
2.67-2.77	2.71+/-0.03(N=11)	0.00-4.93	0.38+/-1.15 (N=18)
Proterozoic felsic igneous		Susceptibility	Average
<u>Density Range</u>	<u>Average Density</u>	<u>Range</u>	<u>Susceptibility</u>
2.59-2.81	2.67+/-0.05(N=52)	0.00-3.18	0.68+/-0.82 (N=104)
Proterozoic mafic igneous		Susceptibility	Average
<u>Density Range</u>	<u>Average Density</u>	<u>Range</u>	<u>Susceptibility</u>
2.70-3.15	2.93+/-0.12(N=20)	0.02-6.37	1.37+/-1.84 (N=22)

Table 2. Density-depth function*

Depth Range	Based on Arizona borehole gravity (Tucci and others, 1982)	Based on Basin & Range (Jachens and Moring, 1990)
0-100 m	-0.67	-0.65
100-200 m	-0.47	-0.65
200-600 m	-0.37	-0.55
600-1200 m	-0.25	-0.35
> 1200 m	-0.25	-0.25

*density contrast (g/cm^3) relative to underlying pre-Cenozoic bedrock.

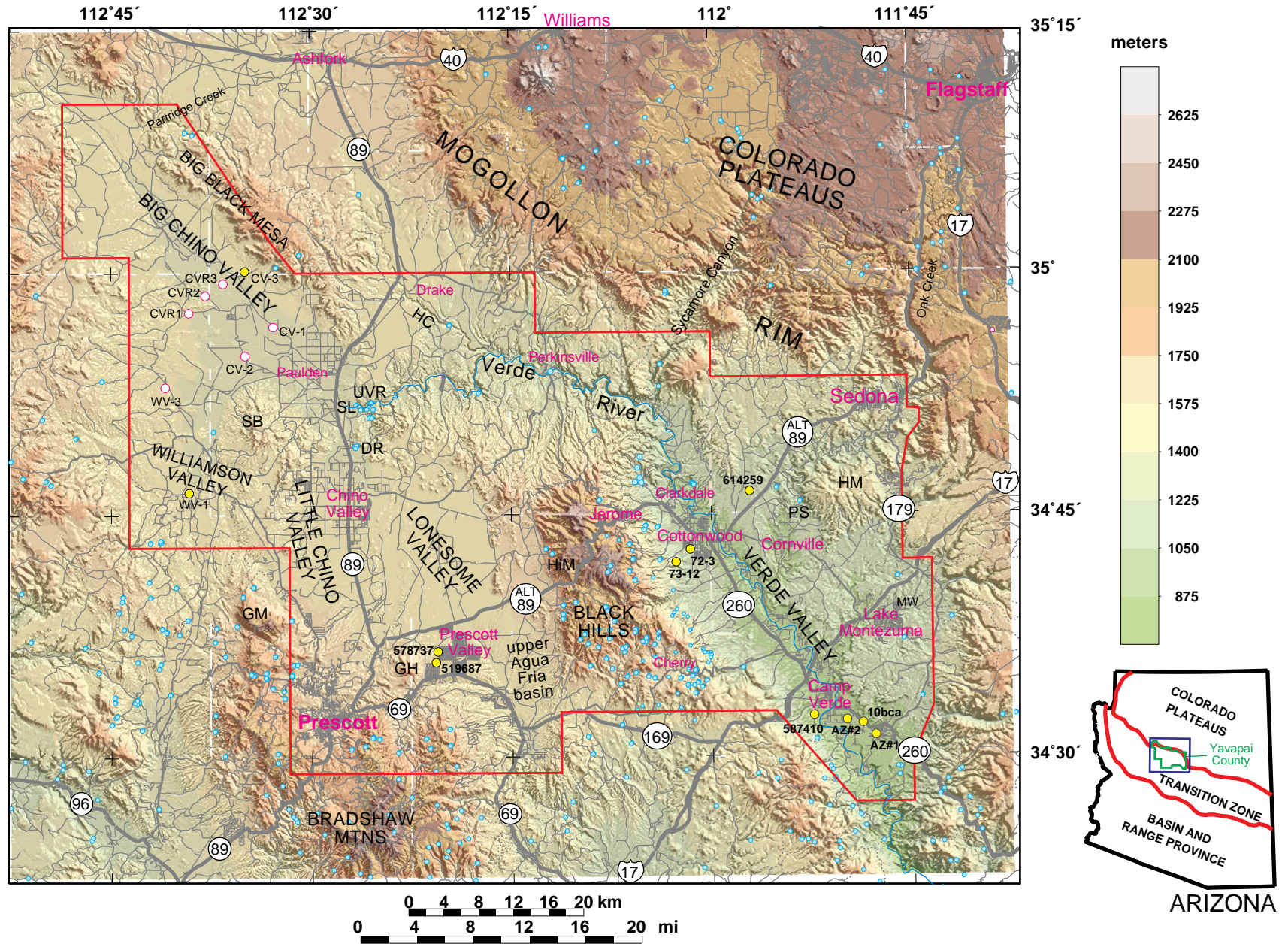


Figure 1. Index map of study area. Red lines outline new aeromagnetic data (Langenheim and others, 2000; 2002). Blue circles denote springs. Towns and cities in magenta lettering. Magenta-rimmed white circles are selected wells that reach pre-Cenozoic bedrock; yellow circles are selected wells that did not reach bedrock. UVR, Upper Verde springs, DR, Del Rio springs; GH, Glassford Hill; GM, Granite Mountain; HC, Hell Canyon; HM, House Mountain; HiM, Hickey Mountain; MW, Montezuma Well; PS, Page Springs; SB, Sullivan Buttes; SL, Sullivan Lake.

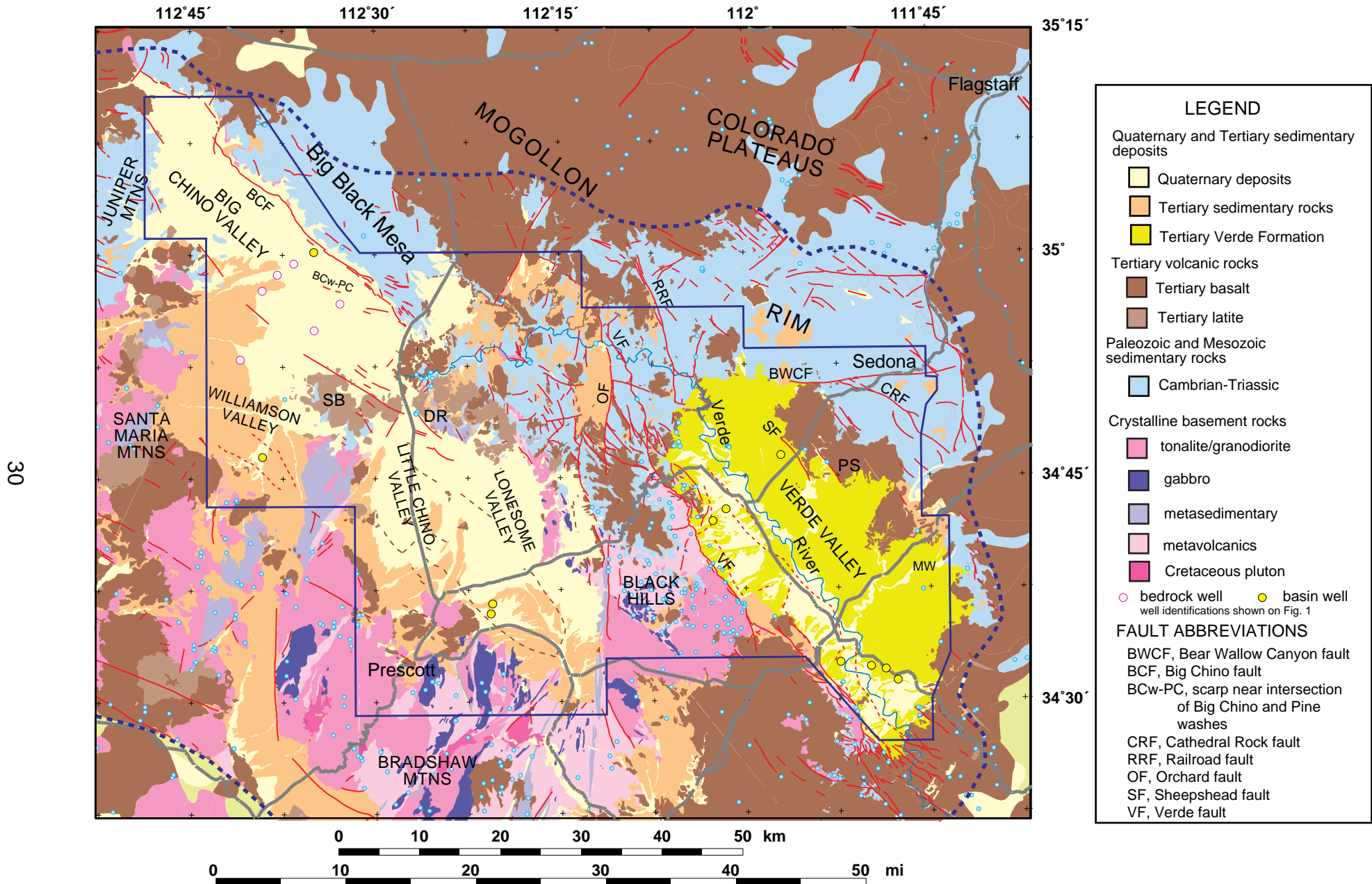


Figure 2. Simplified geologic map of the Yavapai County study area (from DeWitt and others, in press). Geology outside of thick dotted blue line from Reynolds (1988) and Richard and Kneale (1993). See Figure 1 for explanation of abbreviations. Dark blue outlines aeromagnetic survey boundary. Springs are blue circles. Heavy gray lines are highways. Solid red lines are faults from Twenter and Metzger (1963), Owens-Joyce and Bell (1983), Pearthree (1998), and DeWitt and others, in press. Dashed red lines are inferred faults from analysis of gravity data from this study; dashed brown lines are faults located by well and magnetic data.

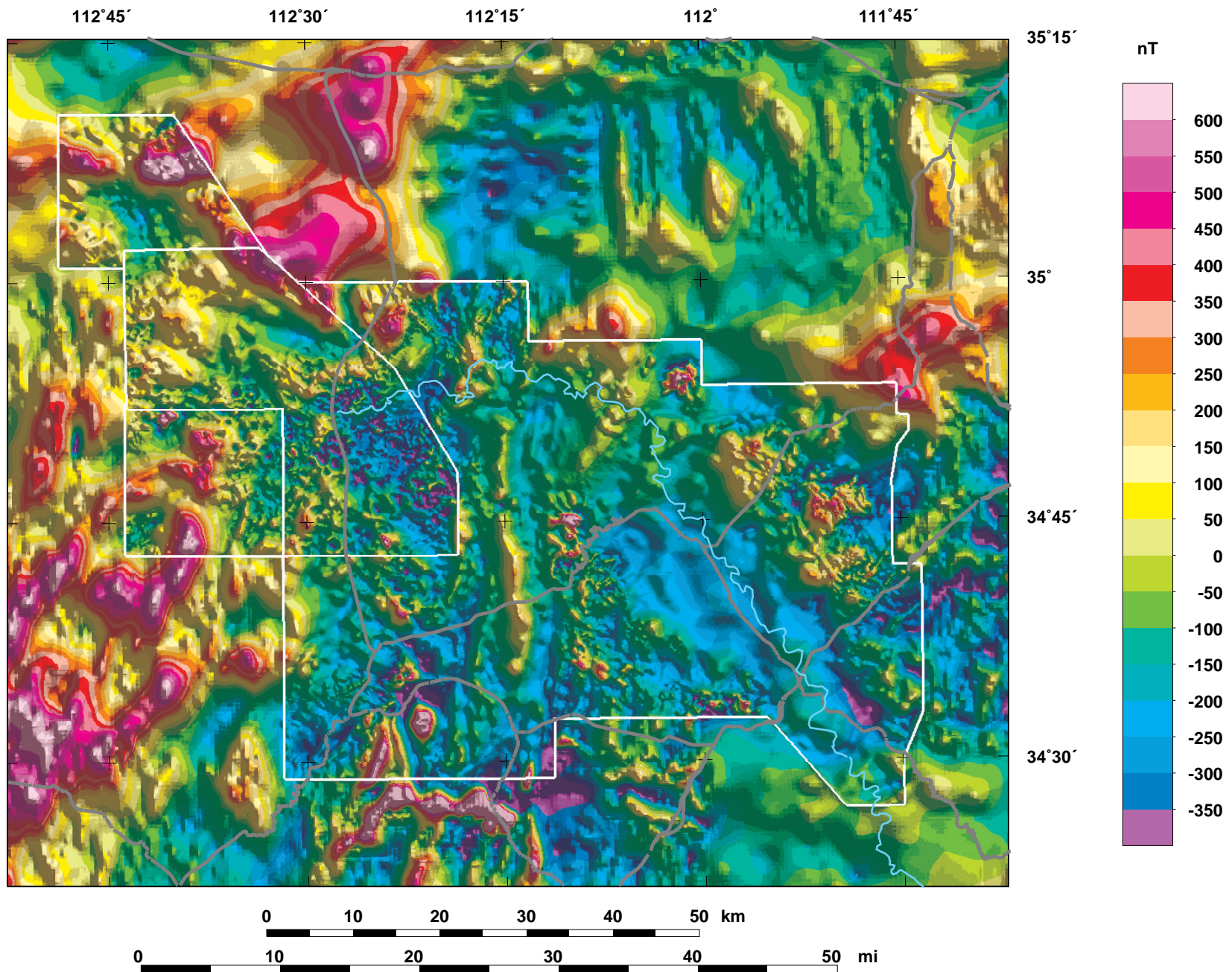


Figure 3. Aeromagnetic anomaly map (reduced to pole). White lines mark boundaries of high-resolution aeromagnetic data collected for this study. Gray lines are highways; blue line is Verde River.

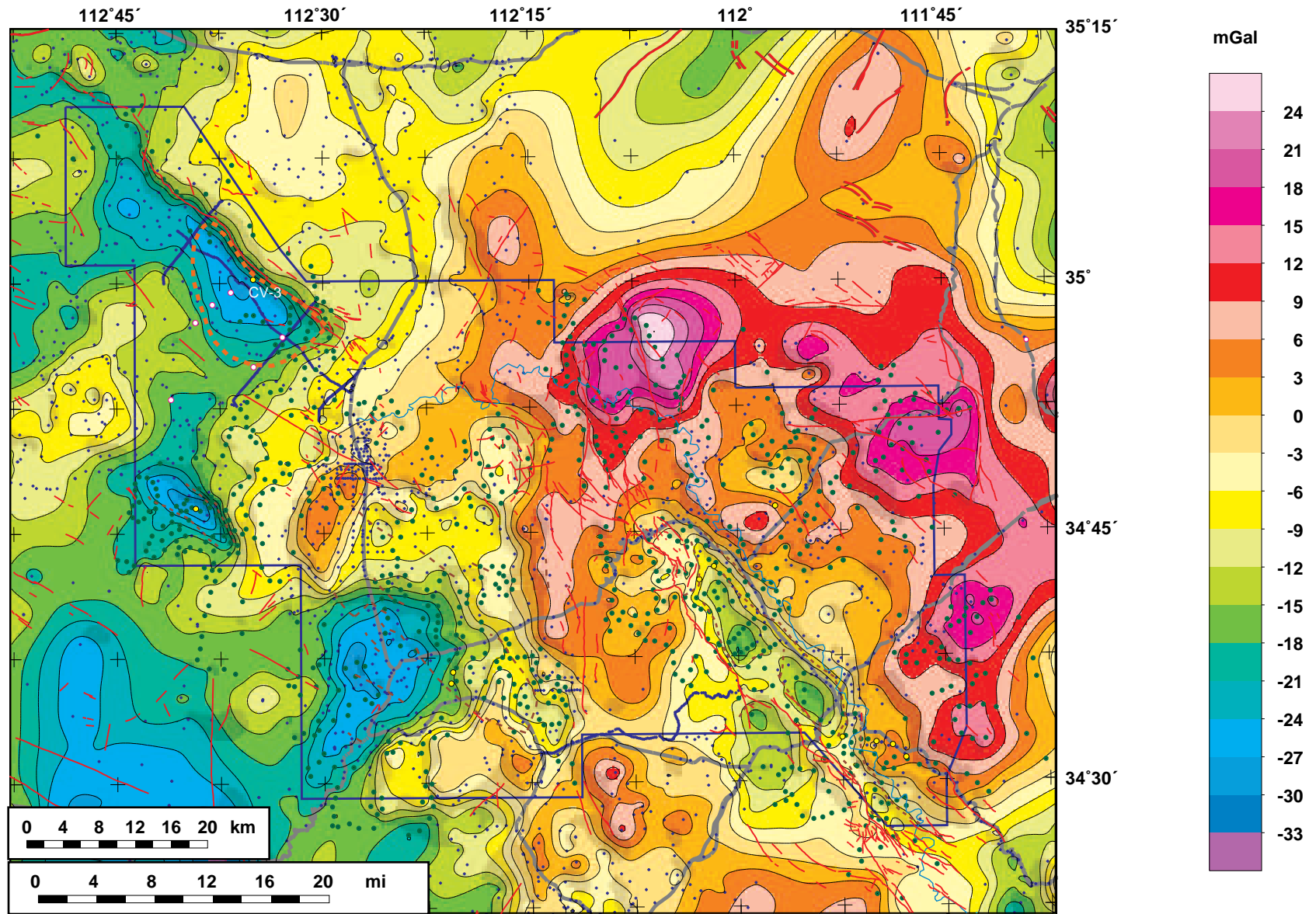


Figure 4. Isostatic gravity anomaly map. Blue line marks extent of high-resolution aeromagnetic data. Gray lines are highways. Dark green circles are gravity data collected for this study; blue dots are previously collected data. Red lines are faults from DeWitt and others (in press). Dashed brown lines, faults inferred from well, magnetic and gravity data. Dashed orange line is extent of fine-grained basin fill in Big Chino Valley from Schwab (1995).

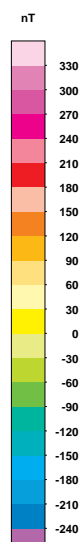
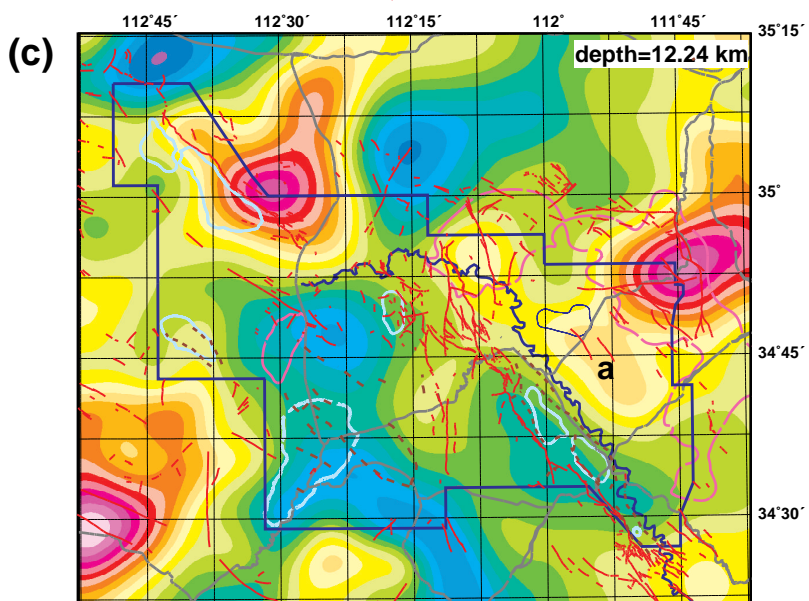
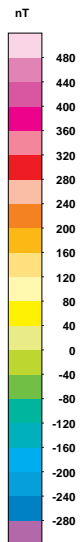
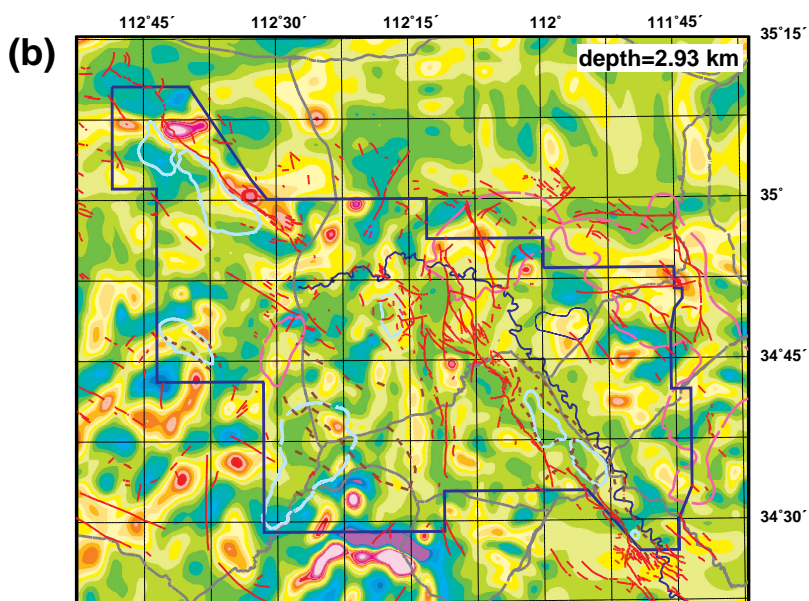
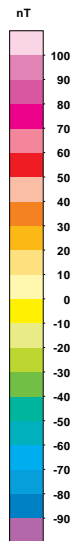
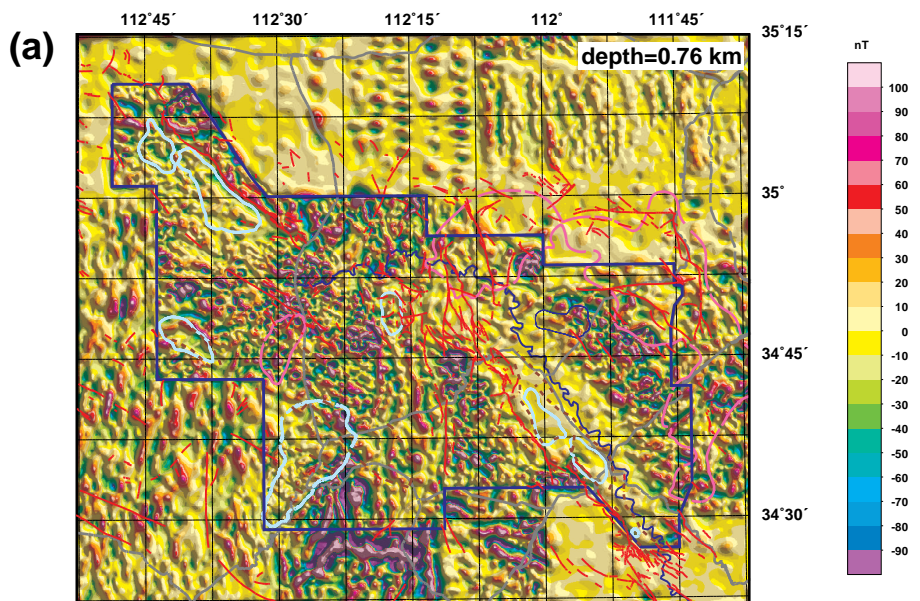


Figure 5. Match-filtered aeromagnetic data. (a) data filtered to enhance veryshallow magnetic sources (< 1 km); (b) data to enhance deeper sources (~2-3 km); (c) data to enhance deep sources (~10 km). Blue line is extent of high-resolution aeromagnetic data. Pale blue lines are gravity lows; pink lines are gravity highs. "a" is a feature discussed in text. Red lines, faults from DeWitt and others (in press); dashed brown lines, faults inferred from geophysical and well data.

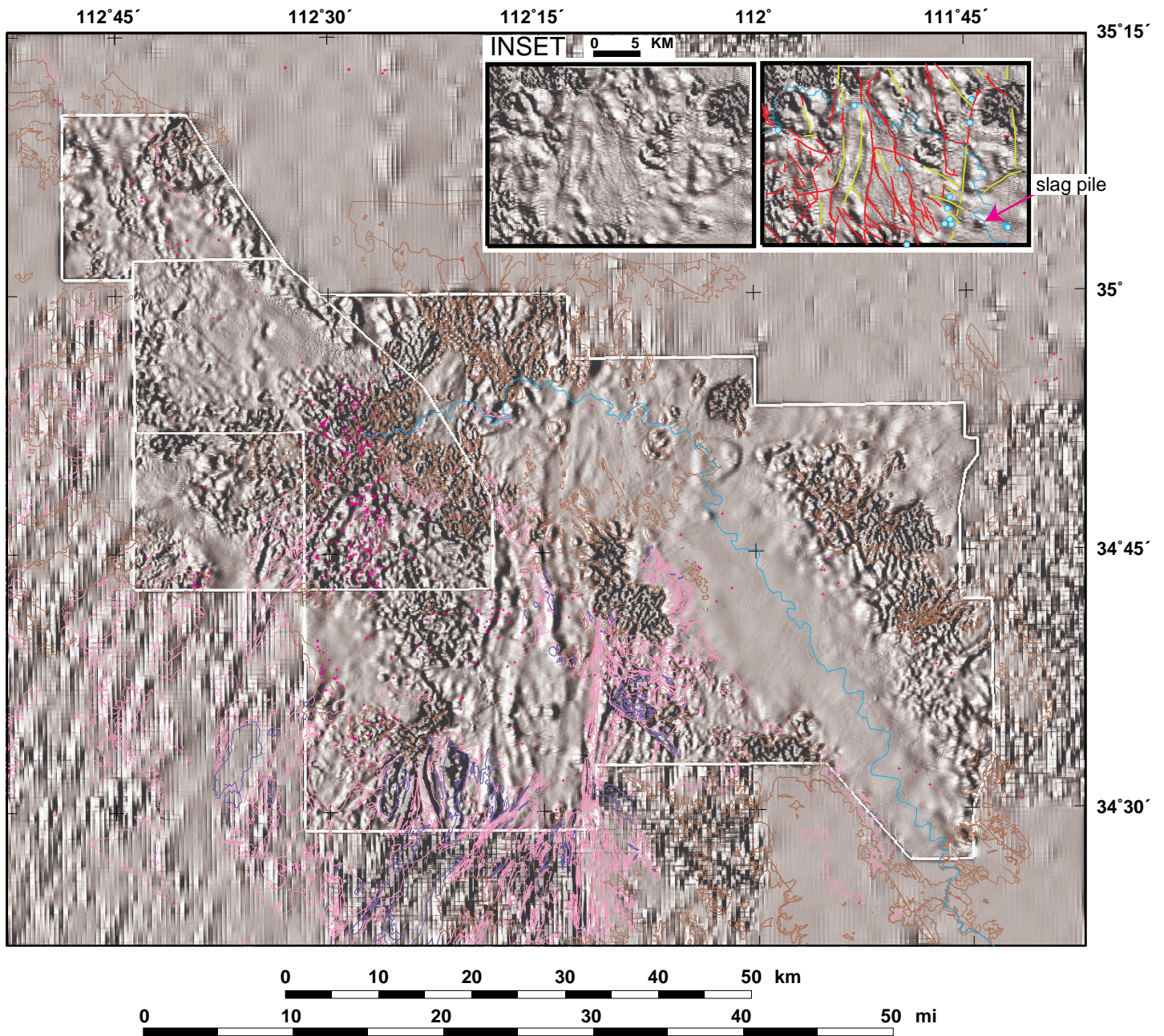


Figure 6. First vertical derivative of the aeromagnetic field. Brown colors indicate where Tertiary volcanic rocks are exposed; pink and purple show where Proterozoic rocks are exposed. Magenta crosses are wells that reach Tertiary volcanic rocks. Blue line is the Verde River. Smooth character of the field outside the extent of high-resolution data (white lines) may reflect lack of resolution from older data. Inset shows area north of Clarkdale with mapped faults (red) and inferred faults (yellow) from subtle magnetic anomalies primarily over Paleozoic sedimentary rocks.

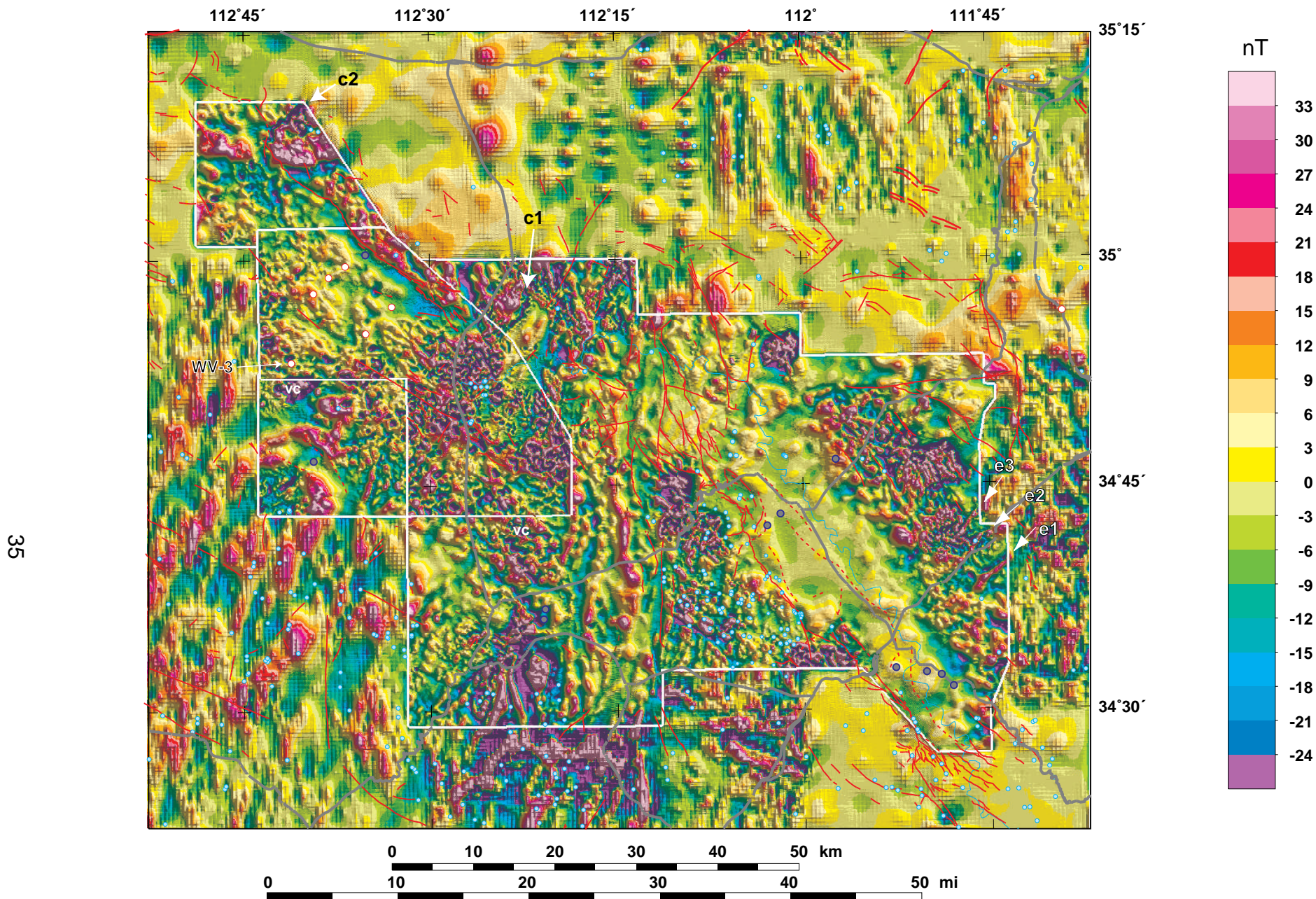


Figure 7. Reduced to pole aeromagnetic data filtered to enhance shallow magnetic sources by subtraction of an upward continued field (100 m). White lines mark extent of new high-resolution aeromagnetic surveys. Blue line is Verde River. Thick gray lines are major highways. Red-rimmed white circles are deep wells that reach pre-Cenozoic bedrock; blue-rimmed gray circles are wells greater than 300 m that do not. Red lines are faults from DeWitt and others (in press); dashed red lines are faults inferred from geophysical and well data. Blue circles are springs.

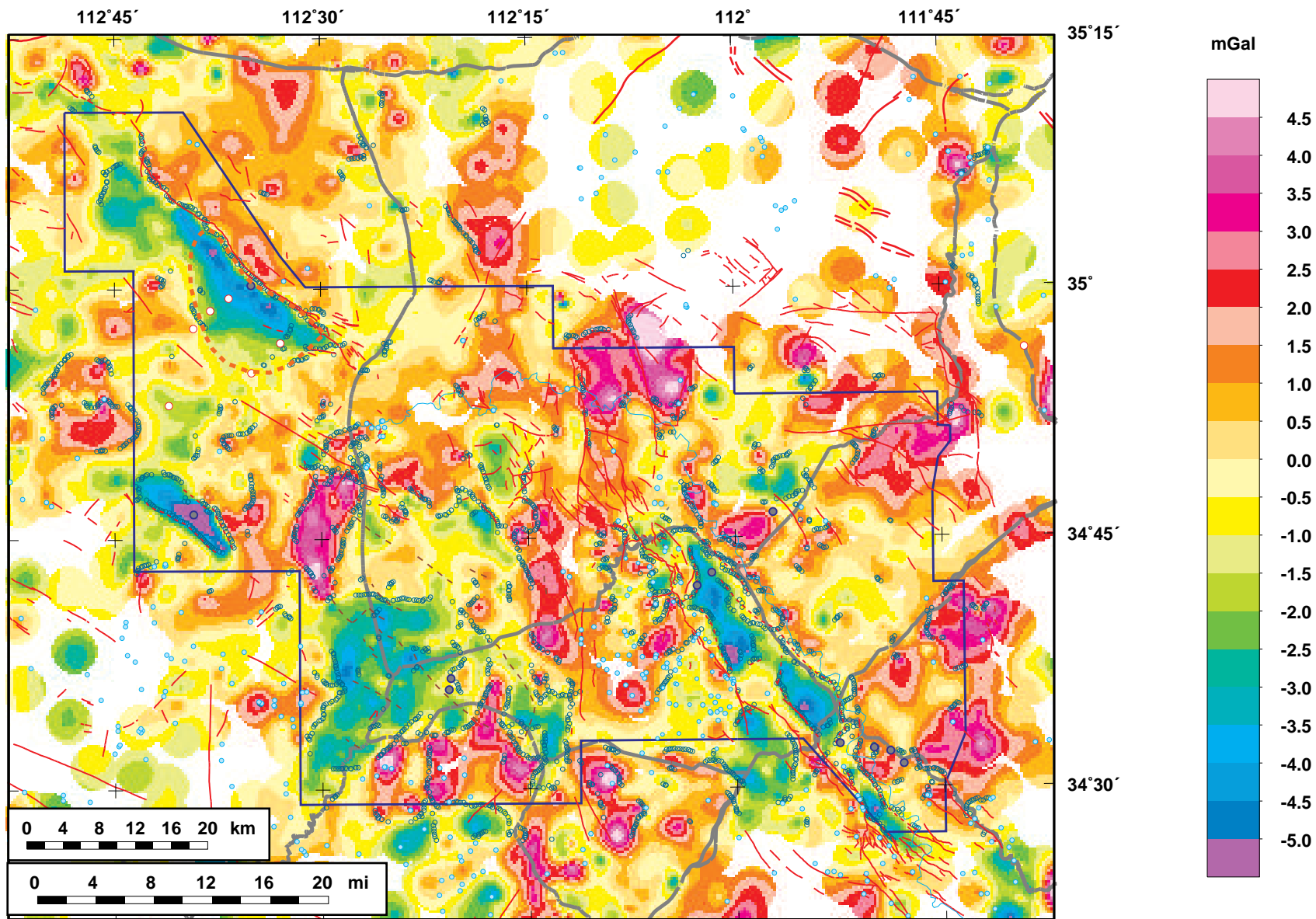


Figure 8. Residual isostatic gravity map. Colored areas within map are gravity values controlled by gravity data within 2.5 km radius of a gravity measurement. Purple line marks extent of high-resolution aeromagnetic data. Light blue line shows the course of the Verde River. Gray lines are highways. Dark blue circles are density boundaries from horizontal gradient method. Red lines, faults from DeWitt and others (in press); brown-dotted and red-dashed lines, faults inferred from well data and gravity gradients, respectively. Orange dashed line is extent of fine-grained deposit in Big Chino Valley from Schwab (1995). Light blue circles are springs.

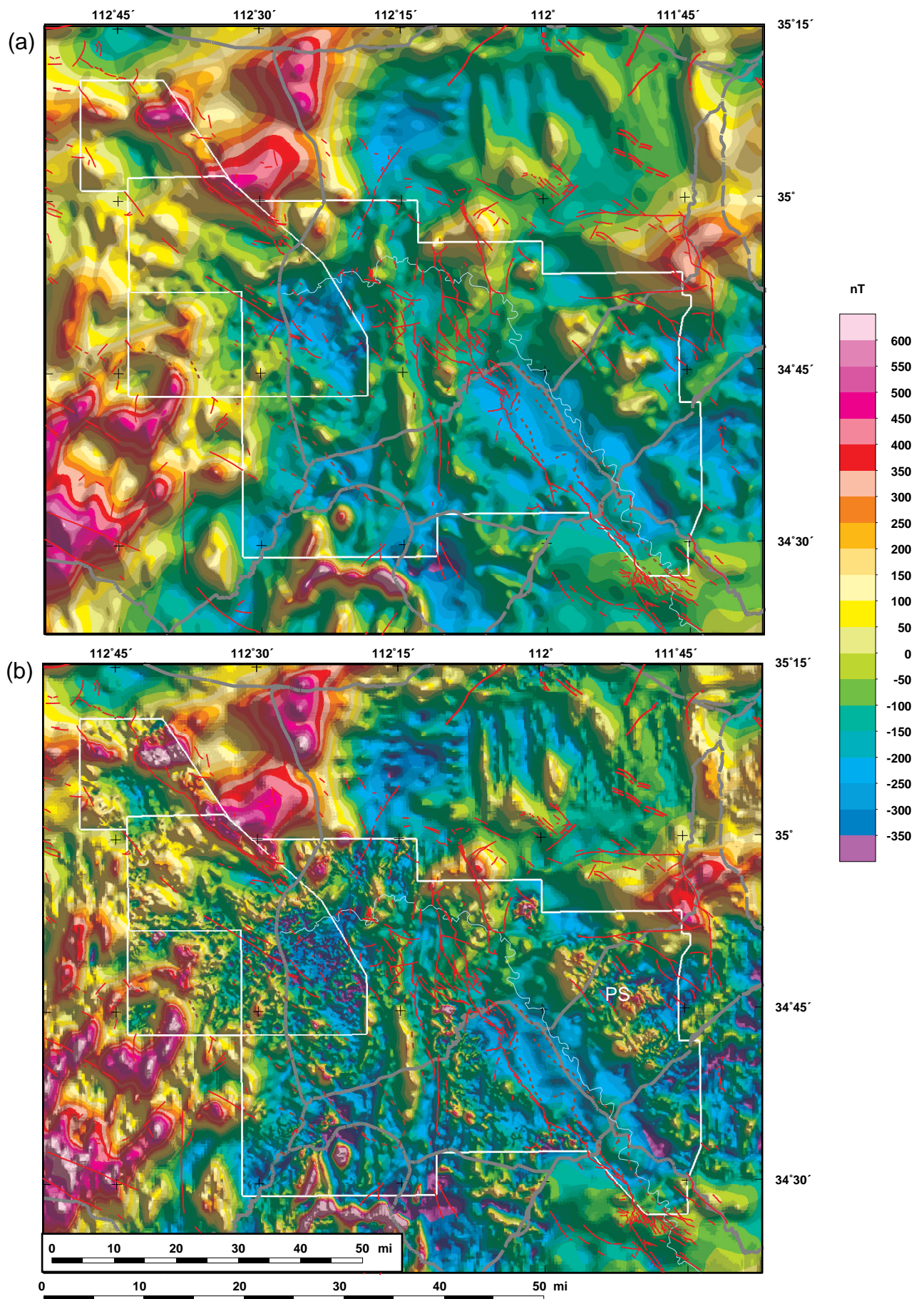


Figure 9. (a) Aeromagnetic map upward continued 750 m, (b) Aeromagnetic map reduced to pole. White lines mark boundaries of high-resolution aeromagnetic data collected for this study. Gray lines are highways; blue line is Verde River. Red lines, faults from DeWitt and others (in press); brown dashed lines are inferred from geophysical and well data.

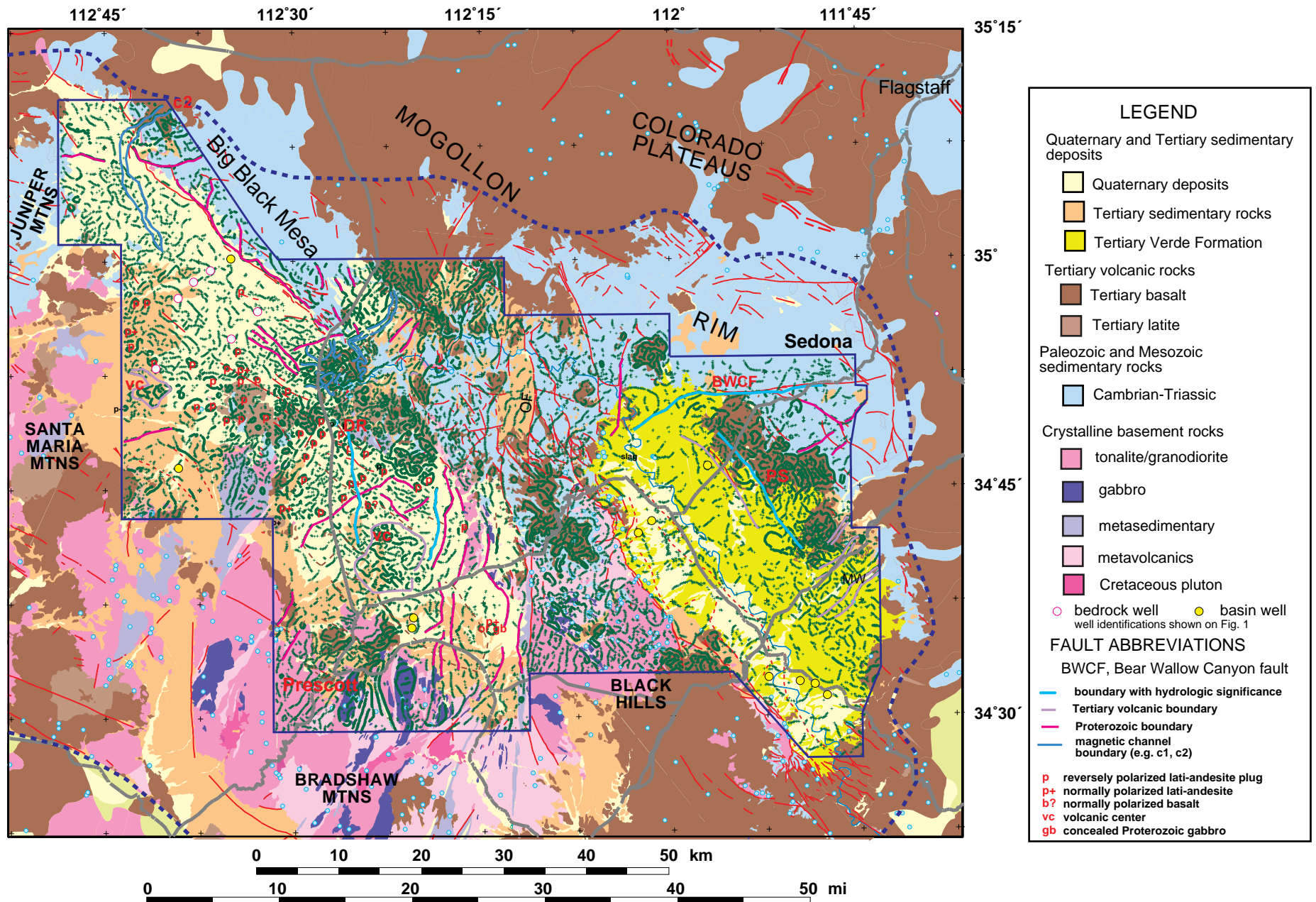


Figure 10. Magnetization boundaries shown by green dots on simplified geologic map of the Yavapai County study area (from DeWitt and others, in press). Geology outside of thick dotted blue line from Reynolds (1988) and Richard and Kneale (1993). See Figure 1 and 2 for explanation of abbreviations and symbols.

AVERAGE DENSITY OF QUATERNARY AND TERTIARY SEDIMENTARY ROCKS
(g/cm³)

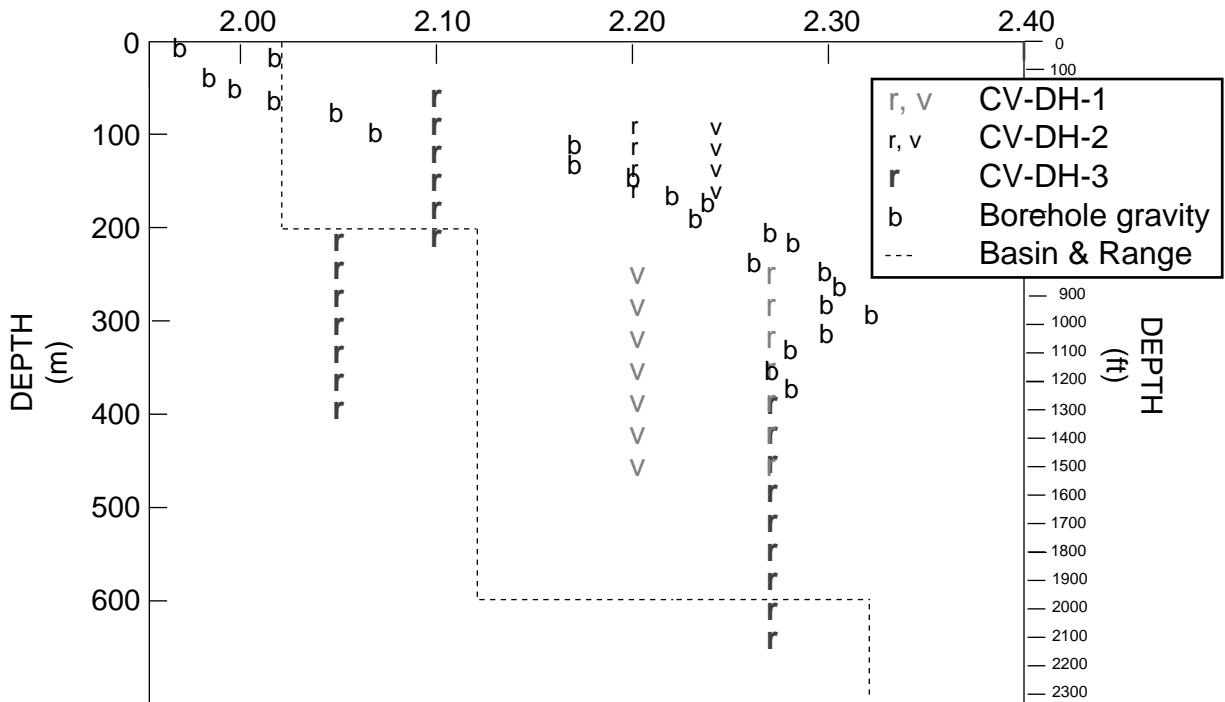


Figure 11. Average densities of Quaternary and Tertiary sedimentary rocks derived from various methods and modified from Langenheim and others (2005). r, derived from electrical resistivity; v, derived from seismic velocity; b, from borehole gravity of Tucci and others (1982; their figure 3); dashed line, density-depth function derived from borehole gravity results of Basin and Range province (Jachens and Moring, 1990).

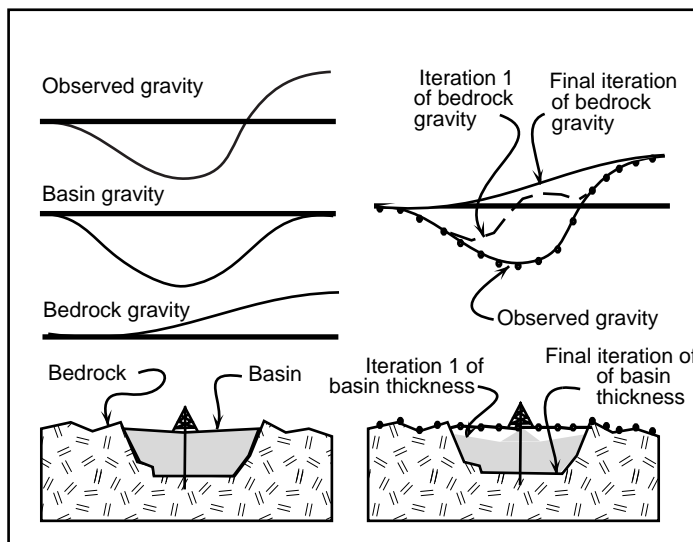


Figure 12. Schematic representation of basin-bedrock separation.

a) Basin and Range density-depth function

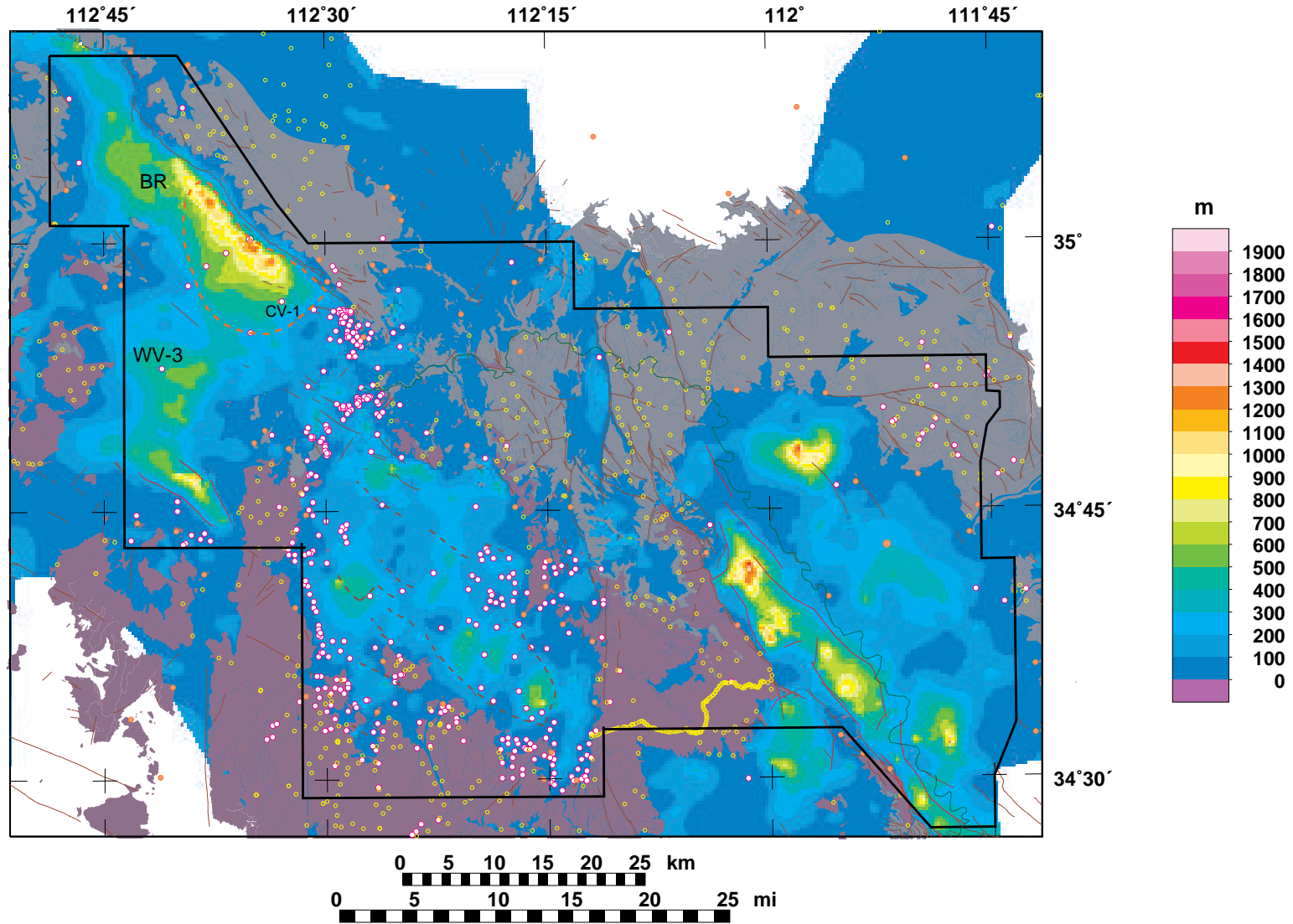


Figure 13. Basin thickness models based on (a) basin and range density-depth function (Jachens and Moring, 1990) and (b) Tucci and others (1982) density-depth function. Yellow circles are gravity stations measured on bedrock; magenta-rimmed white circles are wells that reach bedrock and were used in the gravity inversion; orange circles are additional inferred bedrock gravity information. Light gray areas are Paleozoic sedimentary rocks; dark gray are Proterozoic basement rocks. BR is bedrock ridge. c) comparison of the predicted basin thickness with actual basin thickness encountered in wells for an inversion which did not use these wells as constraints and inversion shown in a).

b) Tucci density-depth function

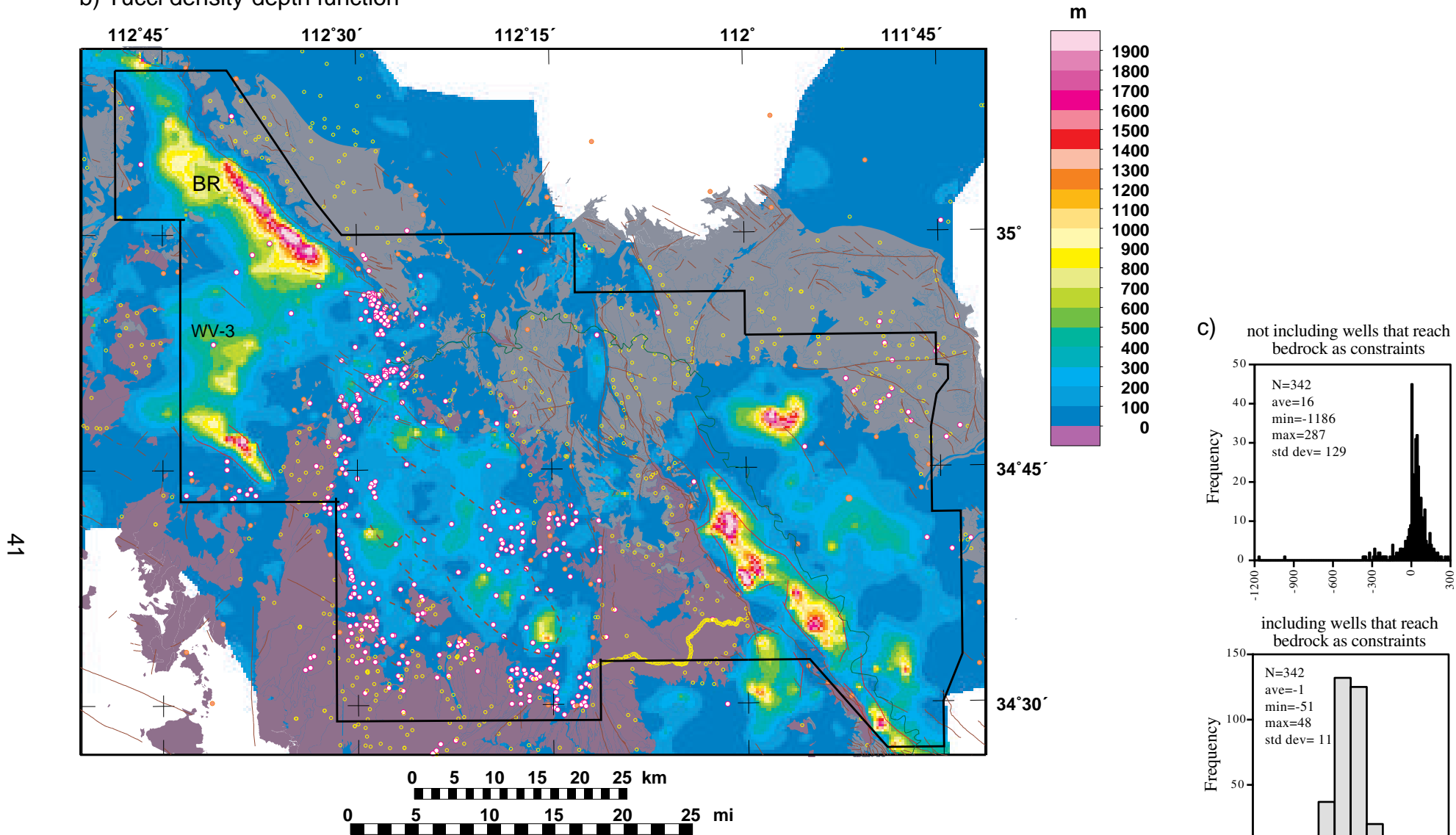


Figure 13. Basin thickness models based on (a) basin and range density-depth function (Jachens and Moring, 1990) and (b) Tucci and others (1982) density-depth function. Yellow circles are gravity stations measured on bedrock; magenta-rimmed white circles are wells that reach bedrock and were used in the gravity inversion; orange circles are additional inferred bedrock gravity information. Light gray areas are Paleozoic sedimentary rocks; dark gray are Proterozoic basement rocks. BR is bedrock ridge. c) comparison of the predicted basin thickness with actual basin thickness encountered in wells for an inversion which did not use these wells as constraints and inversion shown in a).

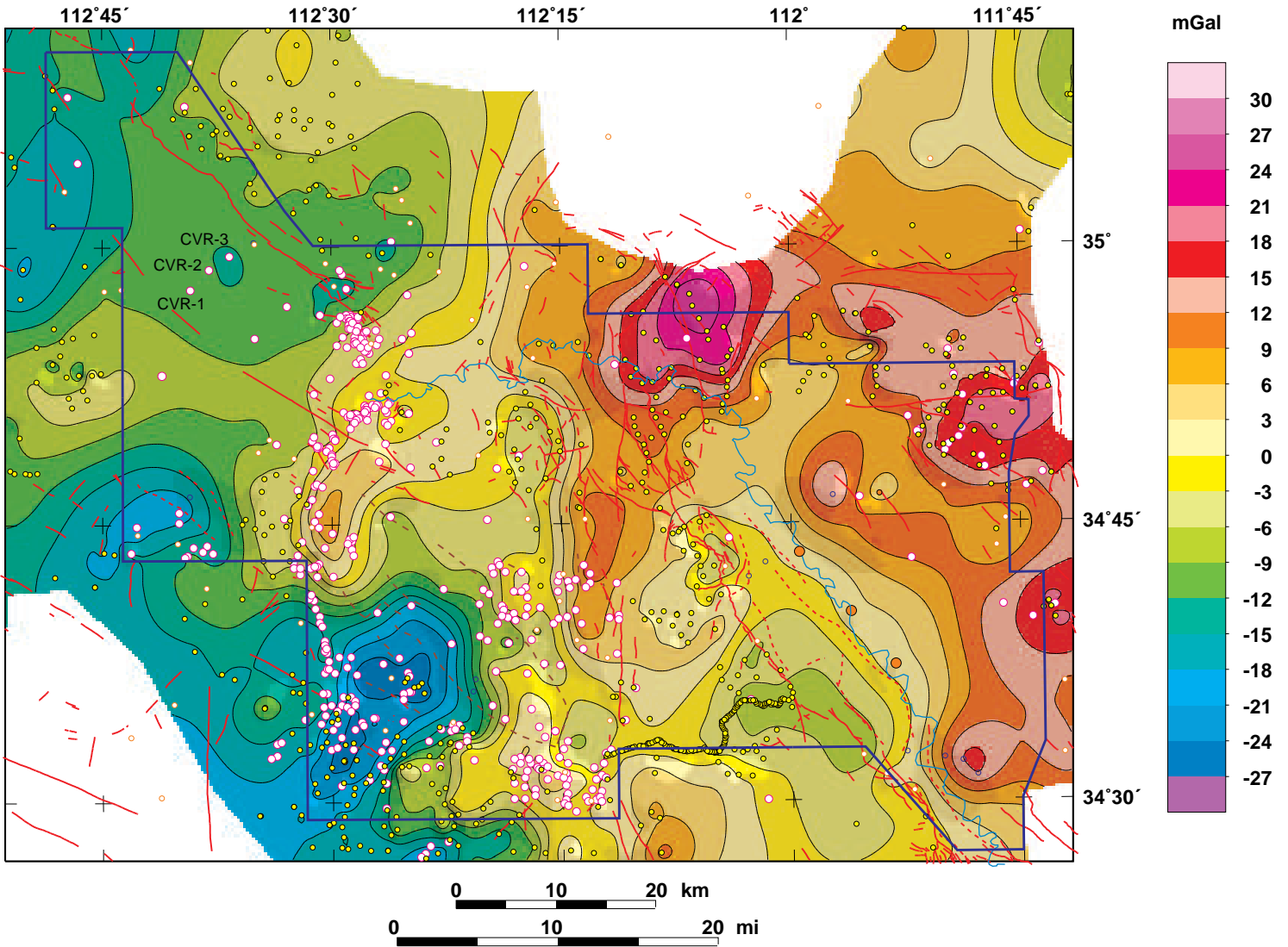


Figure 14. Bedrock gravity field. White circles with red rims are wells that reach bedrock. Yellow circles are gravity stations measured on bedrock. Orange dots are gravity stations measured very close to bedrock or inferred gravity values to help constrain the inversion. Red lines, faults from DeWitt and others (in press). Brown-dotted and red-dashed lines, faults inferred from well and gravity gradients, respectively.

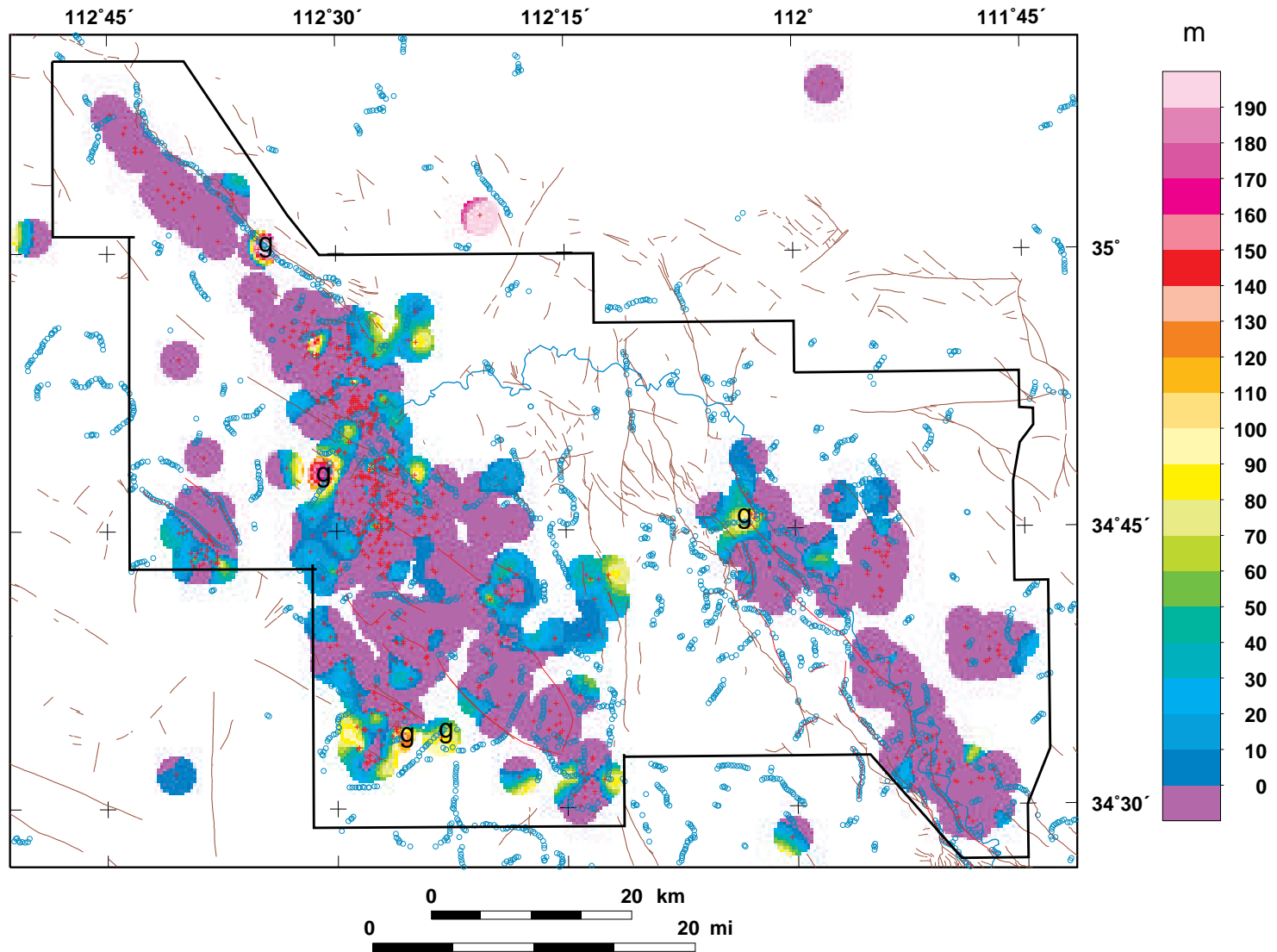


Figure 15. Minimum basin thickness minus predicted basin thickness. Differences greater than 0 indicate that predicted basin surface is too shallow. Red crosses are wells; blue circles are gravity gradients. Brown lines are faults. "g" denotes gravity gradient that may contribute to error in basin thickness estimate.